On Time-Splitting Spectral Approximations for the Schrödinger Equation in the Semiclassical Regime

Weizhu Bao,* Shi Jin,† and Peter A. Markowich‡

*Department of Computational Science, National University of Singapore, Singapore 117543; †Department
of Mathematics, University of Wisconsin-Madison, Madison, Wisconsin 53706; and ‡Institute
of Mathematics, University of Vienna Boltzmanngasse 9, A-1090 Vienna, Austria
E-mail: bao@cz3.nus.edu.sg; jin@math.wisc.edu; peter.markowich@univie.ac.at.

In this paper we study time-splitting spectral approximations for the linear Schrödinger equation in the semiclassical regime, where the Planck constant ε is small. In this regime, the equation propagates oscillations with a wavelength of $O(\varepsilon)$, and finite difference approximations require the spatial mesh size $h = o(\varepsilon)$ and the time step $k = o(\varepsilon)$ in order to obtain physically correct observables. Much sharper mesh-size constraints are necessary for a uniform L^2-approximation of the wave function. The spectral time-splitting approximation under study will be proved to be unconditionally stable, time reversible, and gauge invariant. It conserves the position density and gives uniform L^2-approximation of the wave function for $k = o(\varepsilon)$ and $h = O(\varepsilon)$. Extensive numerical examples in both one and two space dimensions and analytical considerations based on the Wigner transform even show that weaker constraints (e.g., k independent of ε, and $h = O(\varepsilon)$) are admissible for obtaining "correct" observables. Finally, we address the application to nonlinear Schrödinger equations and conduct some numerical experiments to predict the corresponding admissible meshing strategies.   © 2002 Elsevier Science (USA)

1. INTRODUCTION

Many problems of solid physics require the solution of the Schrödinger equation with a small (scaled) Planck constant ε,

$$\varepsilon u_t^\varepsilon - i\frac{\varepsilon^2}{2}\Delta u^\varepsilon + iV(\mathbf{x})u^\varepsilon = 0, \quad t \in \mathbb{R}, \quad \mathbf{x} \in \mathbb{R}^d, \tag{1.1}$$

$$u^\varepsilon(\mathbf{x}, t = 0) = u_0^\varepsilon(\mathbf{x}), \quad \mathbf{x} \in \mathbb{R}^d, \tag{1.2}$$

where $V(\mathbf{x})$ is a given electrostatic potential, $0 < \varepsilon \ll 1$, and $u^\varepsilon = u^\varepsilon(\mathbf{x}, t)$ is the wave function. The wave function is an auxiliary quantity used to compute primary physical quantities such as the position density,

$$n^\varepsilon(\mathbf{x}, t) = |u^\varepsilon(\mathbf{x}, t)|^2, \tag{1.3}$$

the current density,

$$J^\varepsilon(\mathbf{x}, t) = \varepsilon \, \mathrm{Im}(\overline{u^\varepsilon(\mathbf{x}, t)} \nabla u^\varepsilon(\mathbf{x}, t)) = \frac{1}{2i}(\overline{u^\varepsilon} \nabla u^\varepsilon - u^\varepsilon \nabla \overline{u^\varepsilon}), \tag{1.4}$$

where "—" denotes complex conjugation, and the energy density,

$$e^\varepsilon(\mathbf{x}, t) = \frac{\varepsilon^2}{2} |\nabla u^\varepsilon(\mathbf{x}, t)|^2 + V(\mathbf{x})|u^\varepsilon(\mathbf{x}, t)|^2. \tag{1.5}$$

For the definition of general observables, we refer to [9].

It is well known that Eq. (1.1) propagates oscillations of wavelength ε, in space and time, preventing u^ε from converging strongly as $\varepsilon \to 0$. On the other hand, the weak convergence of u^ε is, for example, not sufficient for passing to the limit in the macroscopic densities (1.3)–(1.5). The analysis of the so-called semiclassical limit is a mathematically rather complex issue.

Much progress has been made recently in this area, particularly by the introduction of tools from microlocal analysis, such as defect measures [8], H-measures [19], and Wigner measures [7, 9, 13]. These techniques have provided powerful technical tools for exploiting properties of the Schrödinger equation in the semiclassical limit regime, allowing the passage to the limit $\varepsilon \to 0$ in the macroscopic densities by revealing an underlying kinetic structure. These techniques have not been successfully extended to the semiclassical limit of the (cubically) nonlinear Schrödinger equation, which was solved in the case of one-dimensional defocusing nonlinearity using techniques of inverse scattering [11, 12]. For results regarding the semiclassical limit of the focusing nonlinear Schrödinger equation, see [2, 6, 16].

The oscillatory nature of the solutions of the Schrödinger equation with small ε provides severe numerical burdens. Even for stable discretization schemes (or under mesh size restrictions which guarantee stability), the oscillations may very well pollute the solution in such a way that the quadratic macroscopic quantities and other physical observables come out completely wrong unless the spatial–temporal oscillations are fully resolved numerically, i.e., using many grid points per wavelength of $O(\varepsilon)$. In [14, 15], Markowich *et al.* ultilized the Wigner measure, which was used in analyzing the semiclassical limit for the IVP (1.1) and (1.2), to study the finite difference approximation to the Schrödinger equation with small ε. Their results show that, for the best combination of the time and space discretizations, one needs the following constraint in order to guarantee good approximations to all (smooth) observables for ε small [14, 15]:

$$h = o(\varepsilon), \quad k = o(\varepsilon). \tag{1.6}$$

Failure to satisfy these conditions leads to wrong numerical observables. Much more restrictive conditions are needed to obtain an accurate L^2-approximation of the wave function itself.

In this paper, we study time-splitting spectral approximations for the Schrödinger equation in the semiclassical limit (1.1), (1.2). This approach is based on a time splitting which conserves the total charge and was suggested for nonlinear Schrödinger equations with order 1 Plank constant [18]. The goal of this paper is to understand the resolution capacity of the spectral method for ε-oscillatory solutions. Due to its exponentially high-order accuracy, it is very tempting to believe that the spectral method will allow the meshing size *one order of magnitude larger* than the finite difference methods. Indeed, our classical convergence analysis confirms the meshing strategy,

$$h = O(\varepsilon), \quad k = o(\varepsilon), \tag{1.7}$$

giving L^2-approximation of the wave function. Our numerical experiments in both one and two space dimensions suggest that $k \to 0$ can even be chosen independently of ε, for obtaining "correct" observables, which we prove using the Wigner measure techniques. These results show that the time-splitting spectral method offers compelling advantages over the finite difference methods, especially in higher space dimensions.

The paper is organized as follows. In Section 2 we present the time-splitting spectral approximations for the Schrödinger equation. In Section 3 we prove the convergence of the method under the meshing strategy $h = O(\varepsilon)$ for the case of constant potential using classical error estimates. In this case, there is no error in time discretization. In Section 4 we prove error bounds of the wave function for the case of variable potential under (1.7) and in Section 5 we provide an error analysis of finite difference methods. Section 6 is concerned with the Wigner measure analysis of the spectral-splitting techniques, which give convergence of the observables. In Section 7 numerical results of the time-splitting methods are presented and compared with other methods. We also give an outlook to nonlinear Schrödinger equations, discussing numerical observations which could lead to conjectures about the corresponding meshing strategy. In Section 8 some conclusions are drawn.

2. TIME-SPLITTING SPECTRAL APPROXIMATIONS

In this section we present time-splitting trigonometric spectral approximations of the problem (1.1), (1.2), with periodic boundary conditions. For the simplicity of notation we shall introduce the method for the case of one space dimension ($d = 1$). The analysis in the next section will also focus on the case $d = 1$. Generalizations to $d > 1$ are straightforward for tensor product grids and the results remain valid without modifications. For $d = 1$, the problem becomes

$$\varepsilon u_t^\varepsilon - i \frac{\varepsilon^2}{2} u_{xx}^\varepsilon + i V(x) u^\varepsilon = 0, \quad a < x < b, \quad t > 0, \tag{2.1}$$

$$u^\varepsilon(x, t=0) = u_0^\varepsilon(x), \quad a \le x \le b, \quad u^\varepsilon(a, t) = u^\varepsilon(b, t), \quad u_x^\varepsilon(a, t) = u_x^\varepsilon(b, t), \quad t > 0. \tag{2.2}$$

Clearly, the Schrödinger equation is time reversible, so we could pose Eqs. (2.1) and (2.2) for $t \in \mathbb{R}$.

We choose the spatial mesh size $h = \Delta x > 0$ with $h = (b - a)/M$ for M an even positive integer and the time step $k = \Delta t > 0$, and we let the grid points and the time step be

$$x_j := a + j\,h, \quad t_n := n\,k, \quad j = 0, 1, \ldots, M, \quad n = 0, 1, 2, \ldots.$$

Let $U_j^{\varepsilon,n}$ be the approximation of $u^\varepsilon(x_j, t_n)$ and $\mathbf{u}^{\varepsilon,n}$ be the solution vector at time $t = t_n = nk$ with components $u_j^{\varepsilon,n}$.

The First-Order Time-Splitting Spectral Method (SP1)

From time $t = t_n$ to time $t = t_{n+1}$, the Schrödinger equation (2.1) is solved in two steps. One solves

$$\varepsilon u_t^\varepsilon - i \frac{\varepsilon^2}{2} u_{xx}^\varepsilon = 0 \tag{2.3}$$

for one time step, followed by solving

$$\varepsilon u_t^\varepsilon + i V(x) u^\varepsilon = 0, \tag{2.4}$$

again for one time step. Equation (2.3) will be discretized in space by the spectral method and integrated in time *exactly*. The ODE (2.4) will then be solved exactly. The detailed method is given by

$$U_j^{\varepsilon,*} = \frac{1}{M} \sum_{l=-M/2}^{M/2-1} e^{-i\varepsilon k \mu_l^2 / 2} \hat{U}_l^{\varepsilon,n} e^{i\mu_l(x_j-a)}, \quad j = 0, 1, 2, \ldots, M-1,$$

$$U_j^{\varepsilon,n+1} = e^{-iV(x_j)k/\varepsilon} U_j^{\varepsilon,*}, \tag{2.5}$$

where $\hat{U}_l^{\varepsilon,n}$, the Fourier coefficients of $U^{\varepsilon,n}$, are defined as

$$\mu_l = \frac{2\pi l}{b-a}, \quad \hat{U}_l^{\varepsilon,n} = \sum_{j=0}^{M-1} U_j^{\varepsilon,n} e^{-i\mu_l(x_j-a)}, \quad l = -\frac{M}{2}, \ldots, \frac{M}{2}-1, \tag{2.6}$$

with

$$U_j^{\varepsilon,0} = u^\varepsilon(x_j, 0) = u_0^\varepsilon(x_j), \quad j = 0, 1, 2, \ldots, M. \tag{2.7}$$

Note that the only time discretization error of this method is the splitting error, which is first order in k for any fixed $\varepsilon > 0$. For future reference we define the trigonometric interpolant of a function f on the grid $\{x_0, x_1, \ldots, x_M\}$:

$$f_I(x) = \frac{1}{M} \sum_{l=-M/2}^{M/2-1} \hat{f}_l e^{i\mu_l(x-a)}, \quad \hat{f}_l = \sum_{j=0}^{M-1} f(x_j) e^{-i\mu_l(x_j-a)}, \quad j = -\frac{M}{2}, \ldots, \frac{M}{2}-1. \tag{2.8}$$

The Strang Splitting Spectral Method (SP2)

From time $t = t_n$ to time $t = t_{n+1}$, we split the Schrödinger equation (2.1) via the Strang splitting

$$U_j^{\varepsilon,*} = e^{-iV(x_j)k/2\varepsilon} U_j^{\varepsilon,n}, \quad j = 0, 1, 2, \ldots, M-1,$$

$$U_j^{\varepsilon,**} = \frac{1}{M} \sum_{l=-M/2}^{M/2-1} e^{-i\varepsilon k \mu_l^2/2} \hat{U}_l^{\varepsilon,*} e^{i\mu_l(x_j-a)}, \quad j = 0, 1, 2, \ldots, M-1, \tag{2.9}$$

$$U_j^{\varepsilon,n+1} = e^{-iV(x_j)k/2\varepsilon} U_j^{\varepsilon,**}, \quad j = 0, 1, 2, \ldots, M-1,$$

where $\hat{U}_l^{\varepsilon,*}$, the Fourier coefficients of $U^{\varepsilon,*}$, is defined as

$$\hat{U}_l^{\varepsilon,*} = \sum_{j=0}^{M-1} U_j^{\varepsilon,*} e^{-i\mu_l(x_j-a)}, \quad l = -\frac{M}{2}, \ldots, \frac{M}{2} - 1. \tag{2.10}$$

Again, the overall time discretization error comes solely from the splitting, which is now second order in k for fixed $\varepsilon > 0$.

If $V(x) \equiv V = \text{constant}$, then all the time steps in the above two methods can be combined and the method can be written simply as a one-step method,

$$U_j^{\varepsilon,n} = \frac{1}{M} \sum_{l=-M/2}^{M/2-1} e^{-i(\varepsilon\mu_l^2/2 + V/\varepsilon)t_n} \hat{U}_l^{\varepsilon,0} e^{i\mu_l(x_j-a)}, \tag{2.11}$$

with

$$\hat{U}_l^{\varepsilon,0} = \sum_{j=0}^{M-1} U_j^{\varepsilon,0} e^{-i\mu_l(x_j-a)}, \quad l = -\frac{M}{2}, \ldots, \frac{M}{2} - 1. \tag{2.12}$$

This is the same as discretizing the second-order space derivative in (2.1) by the spectral method, and then solving the resulting ODE system *exactly* to $t = t_n$. Therefore, no time discretization error is introduced and the only error is the spectral error of the spatial derivative.

For benchmark comparisons, we also define other possible schemes. The first is the Crank–Nicolson spectral method (CNSP),

$$\begin{aligned}
\frac{U_j^{\varepsilon,n+1} - U_j^{\varepsilon,n}}{k} &= \frac{i\varepsilon}{4} \left(D_{xx}^s U^{\varepsilon,n+1}\big|_{x=x_j} + D_{xx}^s U^{\varepsilon,n}\big|_{x=x_j} \right) \\
&\quad - \frac{iV(x_j)}{2\varepsilon} \left(U_j^{\varepsilon,n+1} + U_j^{\varepsilon,n} \right), \quad j = 0, 1, \ldots, M-1, \\
U_0^{\varepsilon,n+1} &= U_M^{\varepsilon,n+1}, \quad U_1^{\varepsilon,n+1} = U_{M+1}^{\varepsilon,n+1}, \\
U_j^{\varepsilon,0} &= u_0^\varepsilon(x_j), \quad j = 0, 1, 2, \ldots, M-1,
\end{aligned} \tag{2.13}$$

where D_{xx}^s, a spectral differential operator approximating ∂_{xx}, is defined as

$$D_{xx}^s U|_{x=x_j} = -\frac{1}{M} \sum_{l=-M/2}^{M/2-1} \mu_l^2 \, \hat{U}_l \, e^{i\mu_l(x_j-a)}, \tag{2.14}$$

with

$$\hat{U}_l = \sum_{j=0}^{M-1} U_j e^{-i\mu_l(x_j-a)}, \quad l = -\frac{M}{2}, \ldots, \frac{M}{2} - 1. \tag{2.15}$$

Another scheme for comparison is the Crank–Nicolson finite difference method (CNFD), which is the numerical method most used for the Schrödinger equation. In this method, one

uses the Crank–Nicolson scheme for time derivative and the second-order central difference scheme for spatial derivative. The detailed method is

$$
\begin{aligned}
\frac{U_j^{\varepsilon,n+1} - U_j^{\varepsilon,n}}{k} &= \frac{i\varepsilon}{4h^2}\left(U_{j+1}^{\varepsilon,n+1} - 2U_j^{\varepsilon,n+1} + U_{j-1}^{\varepsilon,n+1} + U_{j+1}^{\varepsilon,n} - 2U_j^{\varepsilon,n} + U_{j-1}^{\varepsilon,n}\right) \\
&\quad - \frac{iV(x_j)}{2\varepsilon}\left(U_j^{\varepsilon,n+1} + U_j^{\varepsilon,n}\right), \quad j = 1, 2, \ldots, M, \\
U_0^{\varepsilon,n+1} &= U_M^{\varepsilon,n+1}, \quad U_{M+1}^{\varepsilon,n+1} = U_1^{\varepsilon,n+1}, \\
U_j^{\varepsilon,0} &= u_0^\varepsilon(x_j), \quad j = 0, 1, 2, \ldots, M.
\end{aligned}
\tag{2.16}
$$

Both CNSP and CNFD, like the SP1 and SP2, are unconditionally stable. This allows the comparison of meshing strategy based solely on resolution capacity without worrying about numerical stability.

We remark that all the difference schemes presented in this paper are time reversible, just as the IVP for the Schrödinger equation. Also, note that a main advantage of the time-splitting methods is their gauge invariance, just as for the Schrödinger equation itself. If the constant α is added to the potential V, then the discrete wave functions $U_j^{\varepsilon,n+1}$ obtained from SP1 and SP2 get multiplied by the phase factor $e^{-i\alpha(n+1)k/\varepsilon}$, which leaves the discrete quadratic observables unchanged. This property does not hold for finite difference schemes.

3. ERROR ESTIMATES FOR CONSTANT POTENTIALS—SP1

Let $\mathbf{u} = (U_0, \ldots, U_{M-1})^T$. Let $\|\times\|_{L^2}$ and $\|\times\|_{l^2}$ be the usual L^2-norm and discrete l^2-norm respectively on the interval (a, b); i.e.,

$$
\|u\|_{L^2} = \sqrt{\int_a^b |u(x)|^2\, dx}, \quad \|\mathbf{u}\|_{l^2} = \sqrt{\frac{b-a}{M}\sum_{j=0}^{M-1} |U_j|^2}.
\tag{3.1}
$$

For the *stability* of the time-splitting spectral approximations SP1 and SP2, with variable potential $V(x)$, we prove the following lemma, which shows that the total charge is conserved.

LEMMA 3.1. *The time-splitting spectral schemes* SP1 (2.5) *and* SP2 (2.9) *are unconditionally stable. In fact, under any mesh size h and time step k,*

$$
\|\mathbf{u}^{\varepsilon,n}\|_{l^2} = \|u_0^\varepsilon\|_{l^2}, \quad n = 1, 2, \ldots,
\tag{3.2}
$$

and consequently

$$
\|u_I^{\varepsilon,n}\|_{L^2} = \|u_I^{\varepsilon,0}\|_{L^2}, \quad n = 1, 2, \ldots.
\tag{3.3}
$$

Here, $u_I^{\varepsilon,n}$ stands for the trigonometric polynomial interpolating $\{(x_0, u_0^{\varepsilon,n}), (x_1, u_1^{\varepsilon,n}), \ldots, (x_M, u_M^{\varepsilon,n})\}$.

Proof. For the scheme SP1 (2.5), noting (2.6) and (3.1), one has

$$
\frac{1}{b-a}\|\mathbf{u}^{\varepsilon,n+1}\|_{l^2}^2 = \frac{1}{M}\sum_{j=0}^{M-1}|U_j^{\varepsilon,n+1}|^2 = \frac{1}{M}\sum_{j=0}^{M-1}\left|e^{-iV(x_j)k/\varepsilon}U_j^{\varepsilon,*}\right|^2 = \frac{1}{M}\sum_{j=0}^{M-1}|U_j^{\varepsilon,*}|^2
$$

$$
= \frac{1}{M}\sum_{j=0}^{M-1}\left|\frac{1}{M}\sum_{l=-M/2}^{M/2-1}e^{-i\varepsilon k\mu_l^2/2}\hat{U}_l^{\varepsilon,n}e^{i\mu_l(x_j-a)}\right|^2
$$

$$
= \frac{1}{M^2}\sum_{l=-M/2}^{M/2-1}\left|e^{-i\varepsilon k\mu_l^2/2}\hat{U}_l^{\varepsilon,n}\right|^2 = \frac{1}{M^2}\sum_{l=-M/2}^{M/2-1}|\hat{U}_l^{\varepsilon,n}|^2
$$

$$
= \frac{1}{M^2}\sum_{l=-M/2}^{M/2-1}\left|\sum_{j=0}^{M-1}U_j^{\varepsilon,n}e^{-i\mu_l(x_j-a)}\right|^2 = \frac{1}{M}\sum_{j=0}^{M-1}|U_j^{\varepsilon,n}|^2
$$

$$
= \frac{1}{b-a}\|\mathbf{u}^{\varepsilon,n}\|_{l^2}^2. \tag{3.4}
$$

Here, we used the identities

$$
\sum_{j=0}^{M-1}e^{i2\pi(k-l)j/M} = \begin{cases} 0, & k-l \neq mM, \\ M, & k-l = mM, \end{cases} \quad m \text{ integer} \tag{3.5}
$$

and

$$
\sum_{l=-M/2}^{M/2-1}e^{i2\pi(k-j)l/M} = \begin{cases} 0, & k-j \neq mM, \\ M, & k-j = mM, \end{cases} \quad m \text{ integer.} \tag{3.6}
$$

For the scheme SP2 (2.9), using (2.10), (3.1), (3.5), and (3.6),

$$
\frac{1}{b-a}\|\mathbf{u}^{\varepsilon,n+1}\|_{l^2}^2 = \frac{1}{M}\sum_{j=0}^{M-1}|U_j^{\varepsilon,n+1}|^2 = \frac{1}{M}\sum_{j=0}^{M-1}\left|e^{-iV(x_j)k/2\varepsilon}U_j^{\varepsilon,**}\right|^2 = \frac{1}{M}\sum_{j=0}^{M-1}\left|U_j^{\varepsilon,**}\right|^2
$$

$$
= \frac{1}{M}\sum_{j=0}^{M-1}\left|\frac{1}{M}\sum_{l=-M/2}^{M/2-1}e^{-i\varepsilon k\mu_l^2/2}\hat{U}_l^{\varepsilon,*}e^{i\mu_l(x_j-a)}\right|^2
$$

$$
= \frac{1}{M^2}\sum_{l=-M/2}^{M/2-1}\left|e^{-i\varepsilon k\mu_l^2/2}\hat{U}_l^{\varepsilon,*}\right|^2 = \frac{1}{M^2}\sum_{l=-M/2}^{M/2-1}|\hat{U}_l^{\varepsilon,*}|^2
$$

$$
= \frac{1}{M^2}\sum_{l=-M/2}^{M/2-1}\left|\sum_{j=0}^{M-1}U_j^{\varepsilon,*}e^{-i\mu_l(x_j-a)}\right|^2 = \frac{1}{M}\sum_{j=0}^{M-1}\left|U_j^{\varepsilon,*}\right|^2
$$

$$
= \frac{1}{M}\sum_{j=0}^{M-1}\left|e^{-iV(x_j)k/2\varepsilon}U_j^{\varepsilon,n}\right|^2 = \frac{1}{M}\sum_{j=0}^{M-1}|U_j^{\varepsilon,n}|^2
$$

$$
= \frac{1}{b-a}\|\mathbf{u}^{\varepsilon,n}\|_{l^2}^2. \tag{3.7}
$$

Thus, the equality (3.2) can be obtained from (3.4) for the scheme SP1 and (3.7) for the

scheme SP2 by induction. Notice that, for every periodic function f, the equality

$$\|f_I\|_{L^2} = \|f\|_{l^2} = \sqrt{\frac{b-a}{M} \sum_{j=0}^{M-1} |f(x_j)|^2} \tag{3.8}$$

holds. Here f_I stands for the trigonometric interpolant of f on $\{x_0, x_1, \ldots, x_M\}$, defined in (2.8). Thus, (3.3) is a combination of (3.2) and (3.8). ∎

To obtain an error estimate, we assume that the function u_0^ε in (1.2) and (2.2) is C^∞ on $\mathbb{R}$ and periodic with period $b - a$. Moreover, we assume that there are positive constants $C_m > 0$, independent of ε, for every integer $m \geq 0$, such that

$$(A) \quad \left\| \frac{d^m}{dx^m} u_0^\varepsilon \right\|_{L^2(a,b)} \leq \frac{C_m}{\varepsilon^m}, \quad \text{for all } m \in \mathbb{N} \cup \{0\}. \tag{3.9}$$

This condition is clearly satisfied by the semiclassical WKB initial data

$$u^\varepsilon(x, 0) = \sqrt{n_0(x)} e^{i S_0(x)/\varepsilon}$$

if n_0 and S_0 are C^∞ on $\mathbb{R}$ and $(b - a)$-periodic.

Now we are ready to prove the following error estimate, which holds for constant potential $V(x) \equiv V = \text{constant}$. In this case, both SP1 and SP2 reduce to (2.11).

THEOREM 3.1. *Let u^ε be the exact solution of (2.1), (2.2), let $V = constant$, and let $u_I^{\varepsilon,n}$ be the trigonometric interpolant of $\mathbf{u}^{\varepsilon,n} = (U_j^{\varepsilon,n})_{j=0}^{M-1}$ as obtained from (2.11). Under assumption (A), we have for all integers $m \geq 1$*

$$\left\| u_I^{\varepsilon,n} - u^\varepsilon(t_n) \right\|_{L^2} \leq D C_m \left(\frac{h}{\varepsilon(b-a)} \right)^m, \tag{3.10}$$

where $D > 0$ is a constant.

Proof. From Theorem 3 in [17] we conclude the estimate

$$\left\| u_I^{\varepsilon,0} - u_0^\varepsilon \right\|_{L^2} \leq D \left(\frac{h}{b-a} \right)^m \left\| \frac{d^m}{dx^m} u_0^\varepsilon \right\|_{L^2} \leq D C_m \left(\frac{h}{\varepsilon(b-a)} \right)^m, \tag{3.11}$$

for $m \geq 1$, where $D > 0$ depends only on $(b - a)$. Since $u_I^{\varepsilon,n}$ is the exact solution of (2.1) (subject to periodic boundary conditions) with $u_I^{\varepsilon,0}$ as initial datum, at $t = t_n$, and since the Schrödinger equation generates a unitary group on the space $L^2(a, b)$, the estimate (3.10) follows. ∎

Remark 3.1. The authors are grateful to J. E. Pasciak, who pointed out the estimate (3.11) to them. This improved the results and helped to simplify the proof of the previous version of the manuscript.

It is important to point out that in the above theorem, the error estimate (3.10) holds for all integers $m > 1$. This is the unique feature of the spectral method not shared by finite difference approximations.

Based on (3.10), we can formulate the following meshing strategy. Let $\delta > 0$ be the desired error bound. Then

$$\left\| u^\varepsilon(t_n) - u_I^{\varepsilon,n} \right\|_{L^2} \leq \delta \tag{3.12}$$

holds if for some $m \geq 1$

$$\frac{h}{\varepsilon} \leq \frac{(b-a)\delta^{1/m}}{(DC_m)^{1/m}}. \tag{3.13}$$

Although the bound on $\frac{h}{\varepsilon}$ obtained in (3.13) is $O(1)$ as $\varepsilon \to 0$ for every fixed $\delta > 0$ and $m \geq 1$, the δ-dependence can be made arbitrarily weak by choosing m sufficiently large. However, increasing m generally restricts $\frac{h}{\varepsilon}$ since C_m may increase (even rapidly) as $m \to \infty$. As is typical for spectral methods, the mesh strategy depends on precise regularity properties of the solution. We mention that the existence of $\gamma > 0$ such that $C_m \gamma^m \to 0$ as $m \to \infty$ implies that the Fourier coefficients $\hat{u}_l^{\varepsilon,0}$ of u_0^ε vanish for $|l| \geq \frac{b-a}{2\pi\varepsilon\gamma}$; i.e., the Fourier series for u_0^ε has only finitely many terms. In this case the meshing strategy (3.13) generates the exact solution of the IVP for the Schrödinger equation by the time-splitting spectral method.

4. ERROR ESTIMATES FOR VARIABLE POTENTIALS—SP1

In this section we establish error estimates for the SP1 in the case of variable potential V. We assume that the solution $u^\varepsilon = u^\varepsilon(x, t)$ of (2.1), (2.2) and the potential $V(x)$ in (2.1) are $C^\infty(\mathbb{R})$ and $(b-a)$-periodic. Moreover, there are positive constants $C_m > 0$, $D_m > 0$, independent of ε, x, t, such that

$$(B) \quad \left\| \frac{\partial^{m_1+m_2}}{\partial x^{m_1} \partial t^{m_2}} u^\varepsilon \right\|_{C([0,T];L^2(a,b))} \leq \frac{C_{m_1+m_2}}{\varepsilon^{m_1+m_2}}, \quad \left\| \frac{d^m}{dx^m} V \right\|_{L^\infty(a,b)} \leq D_m,$$

$$\text{for all } m, m_1, m_2 \in \mathbb{N} \cup \{0\}. \tag{4.1}$$

Thus, we assume that the solution osscillates in space and time with wavelength ε.

Now we are ready to prove the following error estimate, which holds for SP1 with variable potential $V = V(x)$.

THEOREM 4.1. *Let $u^\varepsilon = u^\varepsilon(x, t)$ be the exact solution of (2.1), (2.2) and $\mathbf{u}^{\varepsilon,n}$ be the discrete approximation SP1 given by (2.5). Under assumption (B), and assuming $\frac{k}{\varepsilon} = O(1)$, $\frac{h}{\varepsilon} = O(1)$, we have for all positive integers $m \geq 1$ and $t_n \in [0, T]$ that*

$$\left\| u^\varepsilon(t_n) - u_I^{\varepsilon,n} \right\|_{L^2} \leq G_m \frac{T}{k} \left(\frac{h}{\varepsilon(b-a)} \right)^m + \frac{CTk}{\varepsilon}, \tag{4.2}$$

where C is a positive constant independent of ε, h, k, and m and G_m is independent of ε, h, k.

Proof. First we estimate the local splitting error in (2.3) and (2.4) for (2.1). We define two operators,

$$\mathcal{A} = \frac{ik\varepsilon}{2}\partial_{xx}, \quad \mathcal{B} = -iV(x)k/\varepsilon. \tag{4.3}$$

Let

$$w(x) = e^{\mathcal{B}}e^{\mathcal{A}}u^\varepsilon(\cdot, t_n) \tag{4.4}$$

be the solution obtained from the operator splitting method (without spatial discretization) after one time step with the exact initial data at t_n. Clearly, the exact solution $u^\varepsilon(x, t_{n+1})$ is given by

$$u^\varepsilon(x, t_{n+1}) = e^{\mathcal{A}+\mathcal{B}} u^\varepsilon(\cdot, t_n). \tag{4.5}$$

The analysis of the operator splitting error is classical, and the error results from the non-commutativity of the operators $\mathcal{A}$ and $\mathcal{B}$. When ε is $O(1)$, SP1 gives a first-order error in k. Here it is necessary to understand how the error depends on ε.

By (4.1),

$$\begin{aligned}
(\mathcal{B}\mathcal{A} - \mathcal{A}\mathcal{B})u(x, t) &= \frac{k^2}{2}\partial_{xx}(Vu) - \frac{Vk^2}{2}\partial_{xx}u \\
&= \frac{k^2}{2}u\partial_x^2 V + k^2\partial_x V \partial_x u = O\left(\frac{k^2}{\varepsilon}\right).
\end{aligned} \tag{4.6}$$

A key observation of (4.6) is that the leading order term $\frac{Vk^2}{2}\partial_{xx}u = O(k^2/\varepsilon^2)$ cancels. Consequently, an elementary computation using Taylor expansion on $e^{\mathcal{A}}$, $e^{\mathcal{B}}$ and $e^{\mathcal{A}+\mathcal{B}}$ gives

$$\|u^\varepsilon(t_{n+1}) - w\|_{L^2} = O\left(\frac{k^2}{\varepsilon}\right). \tag{4.7}$$

We have

$$\left\|u^\varepsilon(t_{n+1}) - u_I^{\varepsilon,n+1}\right\|_{L^2} \le \|u^\varepsilon(t_{n+1}) - w\|_{L^2} + \|w - w_I\|_{L^2} + \left\|w_I - u_I^{\varepsilon,n+1}\right\|_{L^2} \tag{4.8}$$

and

$$\begin{aligned}
\left\|w_I - u_I^{\varepsilon,n+1}\right\|_{L^2} &= \|w - u^{\varepsilon,n+1}\|_{l^2} = \left\|e^{\mathcal{B}}(e^{\mathcal{A}}u^\varepsilon(t_n) - e^{\mathcal{A}}u^{\varepsilon,n})\right\|_{l^2} \\
&= \|u^\varepsilon(t_n) - u^{\varepsilon,n}\|_{l^2} = \left\|u^\varepsilon(t_n)_I - u_I^{\varepsilon,n}\right\|_{L^2} \\
&\le \|u^\varepsilon(t_n)_I - u^\varepsilon(t_n)\|_{L^2} + \left\|u^\varepsilon(t_n) - u_I^{\varepsilon,n}\right\|_{L^2}.
\end{aligned} \tag{4.9}$$

For the first equality, we used $\|f\|_{l^2} = \|f_I\|_{L^2}$. For the second, we used the definition of w and the fact that the first step in (2.5) (i.e., the computation of $U_j^{\varepsilon,*}$) is equivalent to the exact solution of the free Schrödinger equation (2.3) with initial datum $u_I^{\varepsilon,n}$. The third equality is based on the conservation property (3.2) and the fourth again on $\|f\|_{l^2} = \|f_I\|_{L^2}$. Thus,

$$\begin{aligned}
&\left\|u^\varepsilon(t_{n+1}) - u_I^{\varepsilon,n+1}\right\|_{L^2} \\
&\quad \le \|u^\varepsilon(t_{n+1}) - w\|_{L^2} + \|w - w_I\|_{L^2} + \|u^\varepsilon(t_n)_I - u^\varepsilon(t_n)\|_{L^2} + \left\|u^\varepsilon(t_n) - u_I^{\varepsilon,n}\right\|_{L^2}.
\end{aligned} \tag{4.10}$$

The first inequality in (3.11) gives

$$\|u^\varepsilon(t_n)_I - u^\varepsilon(t_n)\|_{L^2} \le D\left(\frac{h}{b-a}\right)^m \left\|\frac{d^m}{dx^m}u^\varepsilon(t_n)\right\|_{L^2} \le DC_m\left(\frac{h}{(b-a)\varepsilon}\right)^m, \tag{4.11}$$

where we used the Assumption (B). Analogously,

$$\|w - w_I\|_{L^2} \leq D\left(\frac{h}{b-a}\right)^m \left\|\frac{d^m}{dx^m}w\right\|_{L^2} \leq E_m\left(\frac{h}{(b-a)\varepsilon}\right)^m \qquad (4.12)$$

if $\frac{k}{\varepsilon} = O(1)$, $\frac{h}{\varepsilon(b-a)} = O(1)$. Here we used

$$\left\|\frac{d^m}{dx^m}w\right\|_{L^2} = \left\|\sum_{j=0}^{m}\binom{m}{j}(e^{\mathcal{B}})^{(j)}(e^{\mathcal{A}}u^\varepsilon(t_n))^{(m-j)}\right\|_{L^2}$$

$$\leq \sum_{j=0}^{m}\binom{m}{j}\left\|(e^{\mathcal{B}})^{(j)}\right\|_{L^\infty}\left\|(e^{\mathcal{A}}u^\varepsilon(t_n))^{(m-j)}\right\|_{L^2}. \qquad (4.13)$$

Then, using (4.7), we obtain

$$\|u^\varepsilon(t_{n+1}) - u_I^{\varepsilon,n+1}\|_{L^2}$$

$$\leq F\frac{k^2}{\varepsilon} + E_m\left(\frac{h}{(b-a)\varepsilon}\right)^m + DC_m\left(\frac{h}{(b-a)\varepsilon}\right)^m + \|u^\varepsilon(t_n) - u_I^{\varepsilon,n}\|_{L^2}, \qquad (4.14)$$

assuming $\frac{k}{\varepsilon} = O(1)$, $\frac{h}{\varepsilon(b-a)} = O(1)$. The estimate (4.2) follows by induction. ∎

Again, let $\delta > 0$ be the desired bound such that (3.12) holds. Then the meshing strategy

$$(a) \quad \frac{k}{\varepsilon} = O\left(\frac{\delta}{T}\right), \quad (b) \quad \frac{h}{\varepsilon} = O\left(\frac{\delta^{1/m}}{(G_m)^{1/m}}\left(\frac{k}{T}\right)^{1/m}\right) \qquad (4.15)$$

is suggested by Theorem 4.1, where $m \geq 1$ is an arbitrary integer. Note that the constraint on h is slightly worse than in the constant potential case, due to the factor $(\frac{k}{T})^{1/m}$ appearing in (415b).

Remark 4.1. Our extensive numerical tests and the analysis of Section 6 confirm that the meshing (1.7) is too restrictive for both SP1 and SP2 if only accurate quadratic observables are desired; cf. below.

Remark 4.2. The proof for SP2 involves more complicated calculations and will be omitted here. We believe that one can establish an estimate at least as good as the one for SP1.

5. ERROR ANALYSIS OF CNSP AND CNFD

The analysis of the L^2-error of the CNFD method proceeds by the consistency–stability concept and is completely standard. We extend (2.16) to $[a, b]$ by replacing $U_j^{\varepsilon,n}$ by $u^{\varepsilon,n}(x)$, $U_{j\pm1}^{\varepsilon,n}$ by $u^{\varepsilon,n}(x \pm h)$, and analogously for $U_j^{\varepsilon,n+1}$, $U_{j\pm1}^{\varepsilon,n+1}$. Using (B) we conclude the local discretiztion error of (2.16) by inserting the solution $u^\varepsilon(x, t)$ of (1.1), (1.2) and by Taylor expansion:

$$l_{CNFD}^{\varepsilon,n} = O\left(k^2\|u_{ttt}^\varepsilon\|_{L_t^\infty(L_x^2)}\right) + O\left(h^2\varepsilon\|u_{xxxx}^\varepsilon\|_{L_t^\infty(L_x^2)}\right) = O\left(C_3\frac{k^2}{\varepsilon^3} + C_4\frac{h^2}{\varepsilon^3}\right). \qquad (5.1)$$

Using stability gives

THEOREM 5.1. *The global L^2-error of CNFD is*

$$\|u^\varepsilon(t_n) - u^{\varepsilon,n}\|_{L^2} = O\left(\left(C_3 \frac{k^2}{\varepsilon^3} + C_4 \frac{h^2}{\varepsilon^3}\right) T\right). \tag{5.2}$$

For CNSP we proceed analogously and compute the local discretization error by standard spectral techniques (all of which are already used in Sections 3 and 4 above),

$$l_{CNSP}^{\varepsilon,n} = O\left(k^2 \|u_{ttt}^\varepsilon\|_{L_t^\infty(L_x^2)}\right) + O\left(C_m \left(\frac{h}{(b-a)\varepsilon}\right)^{m-2} \frac{1}{\varepsilon}\right). \tag{5.3}$$

Again, stability gives

THEOREM 5.2. *The global error of CNSP is*

$$\|u^\varepsilon(t_n) - u_I^{\varepsilon,n}\|_{L^2} = O\left(\left(C_3 \frac{k^2}{\varepsilon^3} + C_m \left(\frac{h}{(b-a)\varepsilon}\right)^{m-2} \frac{1}{\varepsilon}\right) T\right). \tag{5.4}$$

Thus, a meshing strategy for CNFD generating a global error of $O(\delta)$ would be

$$k = O\left((\delta\varepsilon^3)^{1/2}\right), \quad h = O\left((\delta\varepsilon^3)^{1/2}\right). \tag{5.5}$$

Less restrictive meshing conditions can be employed if only uniform approximation of the observables is desired [14].

For the CNSP method we conclude the meshing

$$k = O\left((\delta\varepsilon^3)^{1/2}\right), \quad h = O\left(\varepsilon \left(\frac{\varepsilon\delta}{C_m}\right)^{\frac{1}{m-2}}\right), \tag{5.6}$$

for all integers $m > 2$.

We remark that the methods CNFD and CNSP are globally charge conserving, time reversible, but *not* gauge invariant.

6. APPROXIMATION OF OBSERVABLES

Let $f, g \in L^2(\mathbb{R}^d)$. Then the Wigner transform of (f, g) on the scale $\varepsilon > 0$ is defined as the phase–space function:

$$w^\varepsilon(f, g)(x, \xi) = \frac{1}{(2\pi)^d} \int_{\mathbb{R}^d} \bar{f}\left(x + \frac{\varepsilon}{2}\sigma\right) g\left(x - \frac{\varepsilon}{2}\sigma\right) e^{i\sigma\cdot\xi} \, d\sigma \tag{6.1}$$

(cf. [9, 13] for a detailed analysis of the Wigner-transform). It is well known that the estimate

$$\|w^\varepsilon(f, g)\|_{\mathcal{E}^*} \le \|f\|_{L^2(\mathbb{R}^d)} \|g\|_{L^2(\mathbb{R}^d)} \tag{6.2}$$

holds, where $\mathcal{E}$ is the Banach space

$$\mathcal{E} := \left\{\phi \in C_0\left(\mathbb{R}_x^d \times \mathbb{R}_\xi^d\right) : (\mathcal{F}_{\xi \to v}\phi)(x, v) \in L^1\left(\mathbb{R}_v^d; C_0\left(\mathbb{R}_x^d\right)\right)\right\},$$

$$\|\phi\|_{\mathcal{E}} := \int_{\mathbb{R}_v^d} \sup_{x \in \mathbb{R}_x^d} |(\mathcal{F}_{\xi \to v}\phi)(x, v)| \, dv$$

(cf. [13]). $\mathcal{E}^*$ denotes the dual space of $\mathcal{E}$ and $(\mathcal{F}_{\xi \to v}\sigma)(v) := \int_{\mathbb{R}^d_\xi} \sigma(\xi)e^{-iv\cdot\xi}\,d\xi$ denotes the Fourier transform.

Now let $u^\varepsilon(t)$ be the solution of the IVP (1.1), (1.2) and denote

$$w^\varepsilon(t) := w^\varepsilon(u^\varepsilon(t), u^\varepsilon(t)). \tag{6.3}$$

Then w^ε satisfies the Wigner equation

$$w^\varepsilon_t + \xi \cdot \nabla_x w^\varepsilon + \Theta^\varepsilon[V]w^\varepsilon = 0, \quad (x,\xi) \in \mathbb{R}^d_x \times \mathbb{R}^d_\xi, \quad t \in \mathbb{R}, \tag{6.4}$$

$$w^\varepsilon(t=0) = w^\varepsilon(u^\varepsilon_0, u^\varepsilon_0), \tag{6.5}$$

where $\Theta^\varepsilon[V]$ is the pseudo-differential operator,

$$\Theta^\varepsilon[V]w^\varepsilon(x,\xi,t) := \frac{i}{(2\pi)^d}\int_{\mathbb{R}^d_\alpha} \frac{V(x+\frac{\varepsilon}{2}\alpha) - V(x-\frac{\varepsilon}{2}\alpha)}{\varepsilon}\hat{w}^\varepsilon(x,\alpha,t)e^{i\alpha\cdot\xi}\,d\alpha, \tag{6.6}$$

where $\hat{w}^\varepsilon$ stands for the Fourier transform

$$\mathcal{F}_{\xi\to\alpha}w^\varepsilon(x,\cdot,t) := \int_{\mathbb{R}^d_\xi} w^\varepsilon(x,\xi,t)e^{-i\alpha\cdot\xi}\,d\xi.$$

The main advantage of the formulation (6.4), (6.5) is that the semiclassical limit $\varepsilon \to 0$ can easily be carried out. Taking ε to 0 gives the Vlasov equation

$$w^0_t + \xi \cdot \nabla_x w^0 - \nabla_x V(x) \cdot \nabla_\xi w^0 = 0, \quad (x,\xi) \in \mathbb{R}^d_x \times \mathbb{R}^d_\xi, \quad t \in \mathbb{R}, \tag{6.7}$$

$$w^0(t=0) = w^0_I := \lim_{\varepsilon\to 0} w^\varepsilon(u^\varepsilon_0, u^\varepsilon_0) \tag{6.8}$$

(cf. [9, 13]), where

$$w^0 := \lim_{\varepsilon\to 0} w^\varepsilon.$$

Here, the limits hold in an appropriate weak sense (i.e., in $\mathcal{E}^* - \omega^*$) and have to be understood for subsequences $(\varepsilon_{n_k}) \to 0$ of sequence ε_n. We recall that w^0_I, $w^0(t)$ are positive bounded measures on the phase–space $\mathbb{R}^d_x \times \mathbb{R}^d_\xi$.

Now let $a = a(x,\xi)$ be a smooth real-valued phase–space function with sufficient decay as $|x| + |\xi| \to \infty$. Then the self-adjoint pseudo-differential operator

$$A^\varepsilon := a(x, \varepsilon D)^W,$$

where $D := \frac{1}{i}\nabla_x$ and "W" stands for the Weyl-symbol (symmetric generalization; see [9]), is called an observable and

$$E^\varepsilon_a(t) = \int_{\mathbb{R}^d_x} \bar{u}^\varepsilon(t)(a(x,\varepsilon D)^W u^\varepsilon(t))\,dx$$

is its average in the state $u^\varepsilon(t)$. Note that, for example, the position density $n^\varepsilon(t)$ can be defined by

$$\int_{\mathbb{R}^d_x} n^\varepsilon(x,t)\phi(x)\,dx = E^\varepsilon_{\mathbb{1}_{\mathbb{R}^d_\xi}\phi^\varepsilon}(t),$$

where $\phi \in \mathcal{D}(\mathbb{R}^d_x)$ is an arbitrary ξ-independent observable.

A simple computation shows

$$E_a^\varepsilon(t) = \int_{\mathbb{R}_x^d} \int_{\mathbb{R}_\xi^d} w^\varepsilon(x, \xi, t) a(x, \xi) \, dx \, d\xi$$

and consequently, $E_a^\varepsilon(t)$ can be taken to its semiclassical limit

$$\lim_{\varepsilon \to 0} E_a^\varepsilon(t) = \int_{\mathbb{R}_x^d} \int_{\mathbb{R}_\xi^d} w^0(x, \xi, t) a(x, \xi) \, dx \, d\xi.$$

This limit process was considered rigorously in [9, 13].

We remark that the definition and analysis of Wigner transforms can easily be adapted to x-periodic wave functions (by replacing Fourier transforms by Fourier series); for the sake of simplicity we shall, however, consider only the whole space case (1.1), (1.2) here.

Now let $\tilde{u}^\varepsilon(t)$ be an $L^2(\mathbb{R}^d)$-approximation of the wave function $u^\varepsilon(t)$ at time t, uniformly bounded in $L^2(\mathbb{R}^d)$ as $\varepsilon \to 0$. Then we have, denoting $\tilde{w}^\varepsilon(t) = w^\varepsilon(\tilde{u}^\varepsilon(t), \tilde{u}^\varepsilon(t))$,

$$w^\varepsilon(t) - \tilde{w}^\varepsilon(t) = w^\varepsilon(u^\varepsilon(t), u^\varepsilon(t)) - w^\varepsilon(\tilde{u}^\varepsilon(t), \tilde{u}^\varepsilon(t))$$

$$= w^\varepsilon(u^\varepsilon(t) - \tilde{u}^\varepsilon(t), u^\varepsilon(t)) + w^\varepsilon(\tilde{u}^\varepsilon(t), u^\varepsilon(t) - \tilde{u}^\varepsilon(t))$$

due to the bilinearity of the Wigner transform. The estimate (6.2) gives

$$\|w^\varepsilon(t) - \tilde{w}^\varepsilon(t)\|_{\mathcal{E}^*} \leq \left(\|\tilde{u}^\varepsilon(t)\|_{L^2(\mathbb{R}^d)} + \|u^\varepsilon(t)\|_{L^2(\mathbb{R}^d)} \right) \|\tilde{u}^\varepsilon(t) - u^\varepsilon(t)\|_{L^2(\mathbb{R}^d)}$$

$$\leq C \|\tilde{u}^\varepsilon(t) - u^\varepsilon(t)\|_{L^2(\mathbb{R}^d)}. \tag{6.9}$$

Thus, denoting the approximation observable mean value

$$\tilde{E}_a(t) = \int_{\mathbb{R}_x^d} \overline{\tilde{u}^\varepsilon(t)} (a(x, \varepsilon D)^w \tilde{u}^\varepsilon(t)) \, dx = \int_{\mathbb{R}_x^d} \int_{\mathbb{R}_\xi^d} \tilde{w}^\varepsilon(t) a(x, \xi) \, d\xi \, dx,$$

we find

$$|\tilde{E}_a(t) - E_a(t)| \leq \|a\|_{\mathcal{E}} \|\tilde{w}^\varepsilon(t) - w^\varepsilon(t)\|_{\mathcal{E}^*} \leq C \|a\|_{\mathcal{E}} \|\tilde{u}^\varepsilon(t) - u^\varepsilon(t)\|_{L^2(\mathbb{R}^d)}.$$

L^2-approximation of the wave function implies approximation of observable mean values (for sufficiently smooth and decaying observables) of the same order. However, typically, weaker conditions on the mesh parameters h, k suffice to generate accurate observables than necessary for L^2-approximation of $u^\varepsilon(t)$ (cf. [14, 15] for a corresponding analysis of FD-scheme). For example, $\frac{h}{\varepsilon} + \frac{k}{\varepsilon} \to 0$ is sufficient and necessary for the Crank–Nicolson FD-scheme to guarantee that all (smooth and decaying) observables are well approximated. Clearly, this is not sufficient for L^2-approximation of the wave function.

Consider now the first-order time-splitting spectral method (SP1). In the time step $t_n \to t_{n+1}$ the error is induced by the spectral approximation of the interpolation error resulting from the spectral approximation of $u^{\varepsilon,n}$. For the corresponding Wigner transform this error can be estimated using (6.9) and the L^2-estimate of Section 4. Although this might not be optimal, the spatial mesh size condition (4.15b) is surely sufficient to guarantee an $O(\delta)$-error, caused by the spectral approximation, of the observables on the time interval $[0, T]$.

To understand the splitting error we remark that the time splitting (2.3), (2.4) corresponds to the time splitting of the Wigner equation (6.4)

$$w_t^\varepsilon + \xi \cdot \nabla_x w^\varepsilon = 0, \quad t \in [t_n, t_{n+1}] \tag{6.10}$$

followed by

$$w_t^\varepsilon + \Theta^\varepsilon[V]w^\varepsilon = 0, \quad t \in [t_n, t_{n+1}]. \tag{6.11}$$

Clearly, the limit $\varepsilon \to 0$ can be carried out in (6.11) leaving k *fixed* and we obtain the corresponding time splitting of the Vlasov equation (6.7)

$$w_t^0 + \xi \cdot \nabla_x w^0 = 0, \quad t \in [t_n, t_{n+1}] \tag{6.12}$$

followed by

$$w_t^0 - \nabla_x V \cdot \nabla_\xi w^0 = 0, \quad t \in [t_n, t_{n+1}]. \tag{6.13}$$

Note that *no* other error is introduced by the splitting (SP1) since the time integrations are performed *exactly*.

These considerations, which can be made rigorous easily, show that a *uniform* (i.e., *ε-independent*) time-stepping control,

$$k = O(\delta), \tag{6.14}$$

combined with the spectral mesh-size control (415b) gives an $O(\delta)$-error uniformly as $\varepsilon \to 0$ in the Wigner function and consequently in all observable mean values (corresponding to smooth and decaying function $a(x, \xi)$). This strategy, actually confirmed by the numerical experiments carried out in the next section, is clearly superior to FD schemes, which require $\frac{k}{\varepsilon} \to 0$ even for the approximation of observables.

7. NUMERICAL EXAMPLES

In our computations, the initial condition (1.2) is always chosen in classical WKB form

$$u^\varepsilon(\mathbf{x}, t = 0) = u_0^\varepsilon(\mathbf{x}) = \sqrt{n_0(\mathbf{x})} \, e^{iS_0(\mathbf{x})/\varepsilon}, \tag{7.1}$$

with n_0 and S_0 independent of ε, real valued, regular, and with $n_0(\mathbf{x})$ decaying to zero sufficiently fast as $|\mathbf{x}| \to \infty$. We choose an appropriately long interval $[a, b]$ for the computations such that the periodic boundary conditions do not introduce a significant error relative to the whole space problem.

EXAMPLE 1.   The initial condition is taken as

$$n_0(x) = \left(e^{-25(x-0.5)^2}\right)^2, \quad S_0(x) = -\frac{1}{5}\ln\left(e^{5(x-0.5)} + e^{-5(x-0.5)}\right), \quad x \in \mathbb{R}. \tag{7.2}$$

This example was already used in [12, 14]. We solve on the x-interval $[0, 1]$, i.e., $a = 0$ and $b = 1$ with periodic boundary conditions. Let $V(x) = 10$ be a constant potential. Due
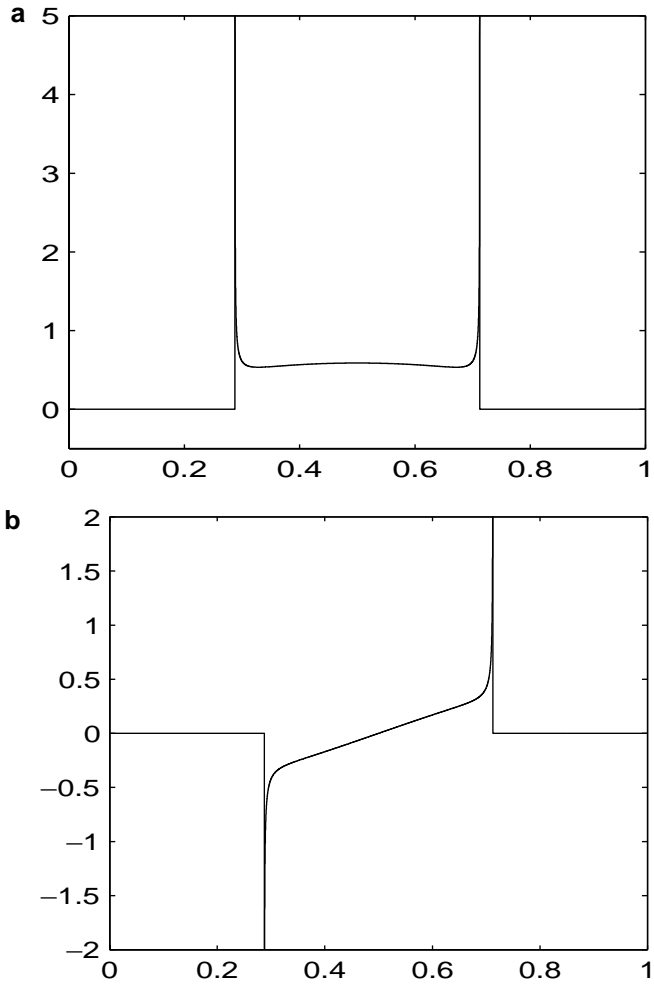
FIG. 1. Weak limits in Example 1 at $t = 0.54$. (a) $n^0(x, 0.54)$; (b) $J^0(x, 0.54)$.

to the compressive initial velocity $\frac{d}{dx}S_0(x)$, caustics will form. The weak limits $n^0(x, t)$, $J^0(x, t)$ of $n^\varepsilon(x, t)$, $J^\varepsilon(x, t)$, respectively, as $\varepsilon \to 0$, given in [12], can be computed by evaluating the zeroth- and first-order velocity moments of the limiting Wigner function for $\varepsilon \to 0$, which solves the Vlasov equation [14]. As a reference we plot them at $t = 0.54$ (after the caustics formed) in Fig. 1.

First, we test the meshing strategy of the time-splitting spectral approximation (2.11) (note that for constant potential SP1 is of course equivalent to SP2). Figure 2 shows the numerical results with different combinations of ε, h. Note that no time-discretization error is introduced for constant potential; i.e., the corresponding discrete wave functions are independent of k at a fixed value $t = t_n$. Thus, we compute the solution in one time step. In Fig. 2 as well as in Figs. 3 and 4 and 6–8, the dotted line is the corresponding weak limit solution and the solid line is the numerically obtained solution. From this figure we can see that, under the meshing strategy
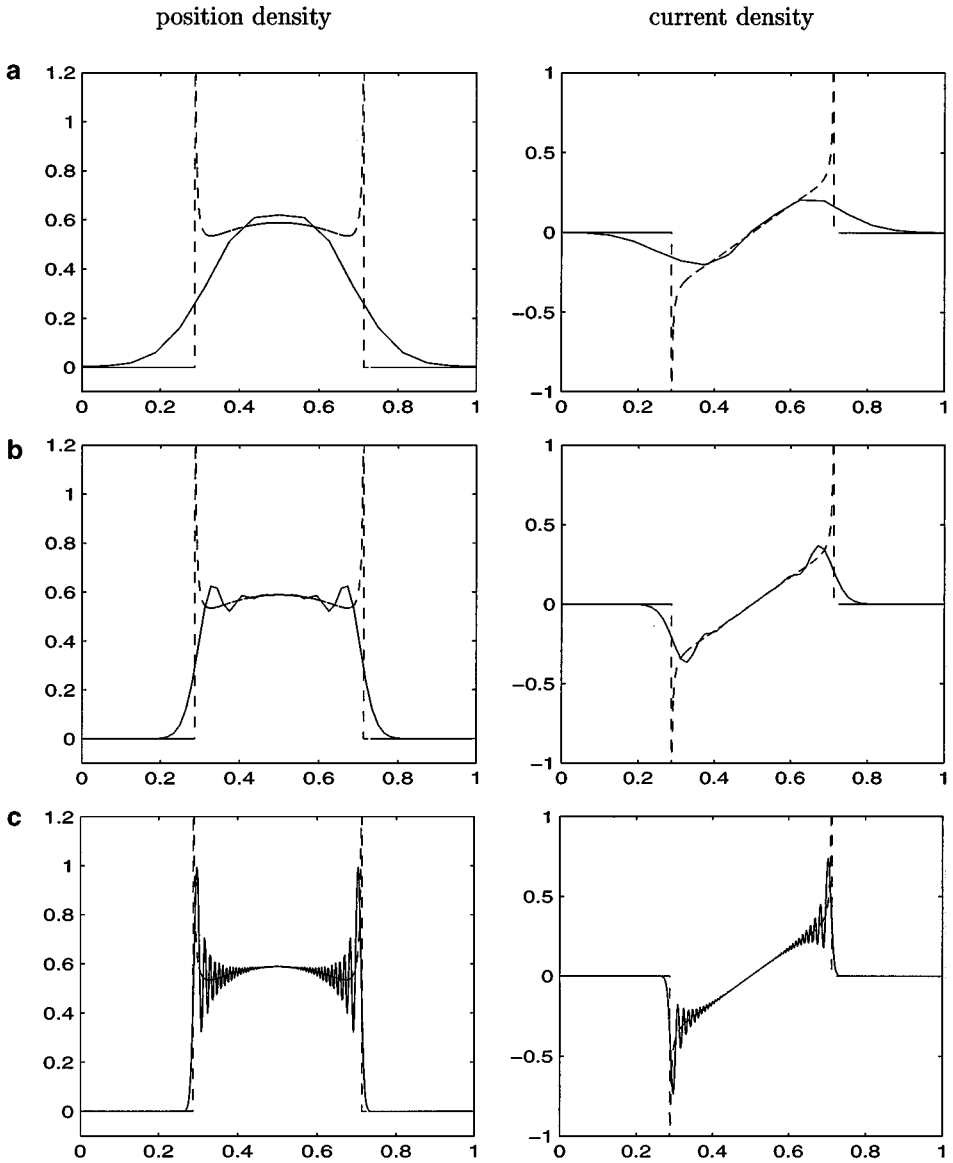
$$\frac{h}{\varepsilon} = O(1), \tag{7.3}$$

position density   current density

FIG. 2. Numerical solutions at $t = 0.54$ in Example 1 by using SP2 (2.9). $V(x) = 10$. (a) $\varepsilon = 0.0256$, $h = \frac{1}{16}$; (b) $\varepsilon = 0.0064$, $h = \frac{1}{64}$; (c) $\varepsilon = 0.0008$, $h = \frac{1}{512}$; (d) $\varepsilon = 0.0001$, $h = \frac{1}{4096}$; (e) $\varepsilon = 0.000025$, $h = \frac{1}{16384}$; (f) $\varepsilon = 0.0000125$, $h = \frac{1}{32768}$.

we observe numerical convergence (in the weak sense) to the limit solution as ε, $h \to 0$.

In order to test the importance of the time discretization, we consider the Crank–Nicolson spectral method (2.13). We choose the same mesh size h, which is the same order as $\varepsilon = 10^{-3}$, and test the effect of different time steps in CNSP. The results are plotted in Fig. 3. One can see that for CNSP, even for $k = 0.0001$, the numerical solution cannot capture the correct weak limit. For $k = 10^{-5}$, CNSP gives a solution comparable to the solution of SP2. Our numerical experiments indicate that the correct meshing strategy for
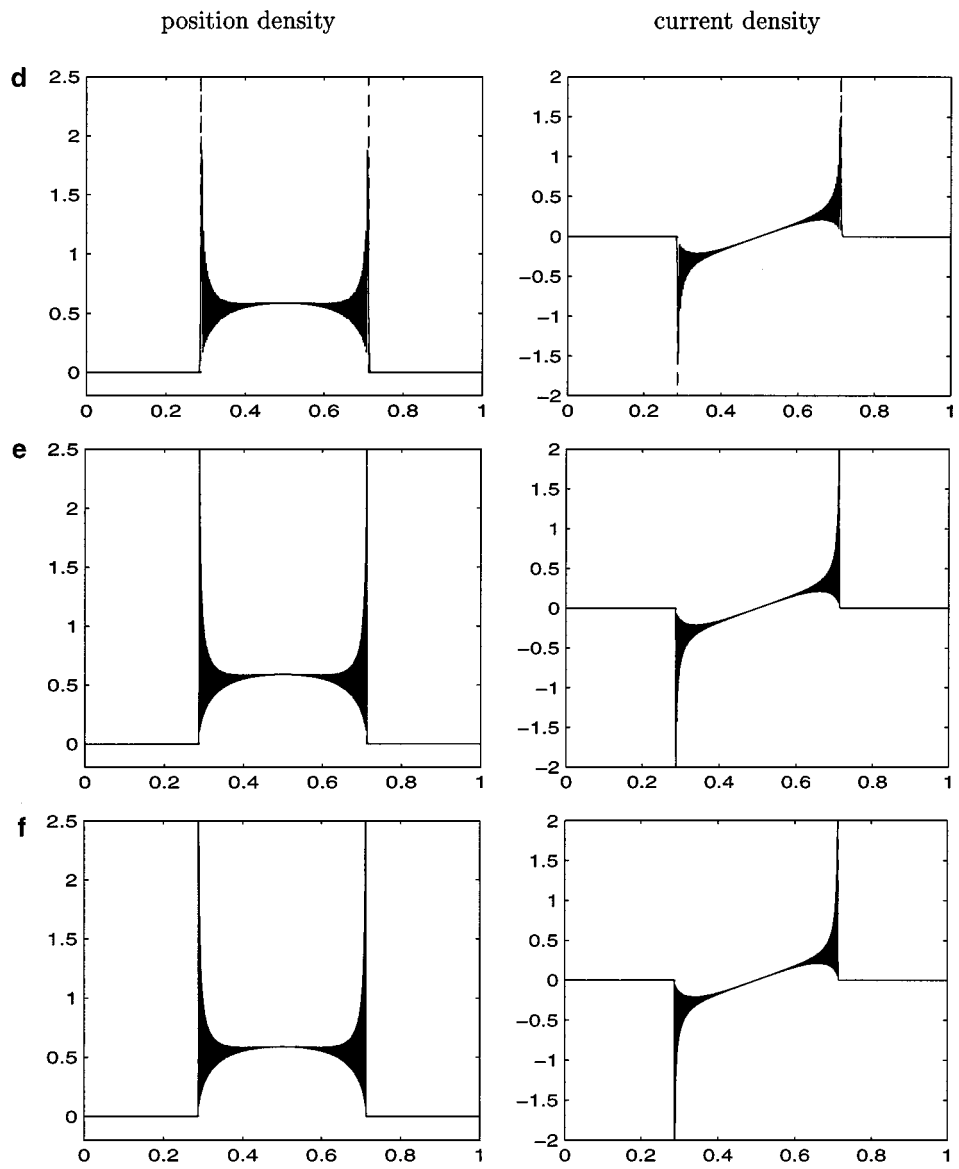
position density   current density

FIG. 2—*Continued*

CNSP is

$$\frac{h}{\varepsilon} = O(1), \quad \frac{k}{\varepsilon} = o(1). \tag{7.4}$$

Third, we compare the difference between the spectral discretization and the finite difference discretization, when in both schemes the same time discretization, namely the Crank–Nicolson method, is used. We shall compare the performance of CNSP with CNFD (2.16). We always choose a very small time step k to eliminate temporal discretization errors. Figure 4 shows the numerical results for different mesh sizes h. It shows that, when the time step resolves the semiclassical scale ε, the spectral method allows a mesh size h

position density   current density
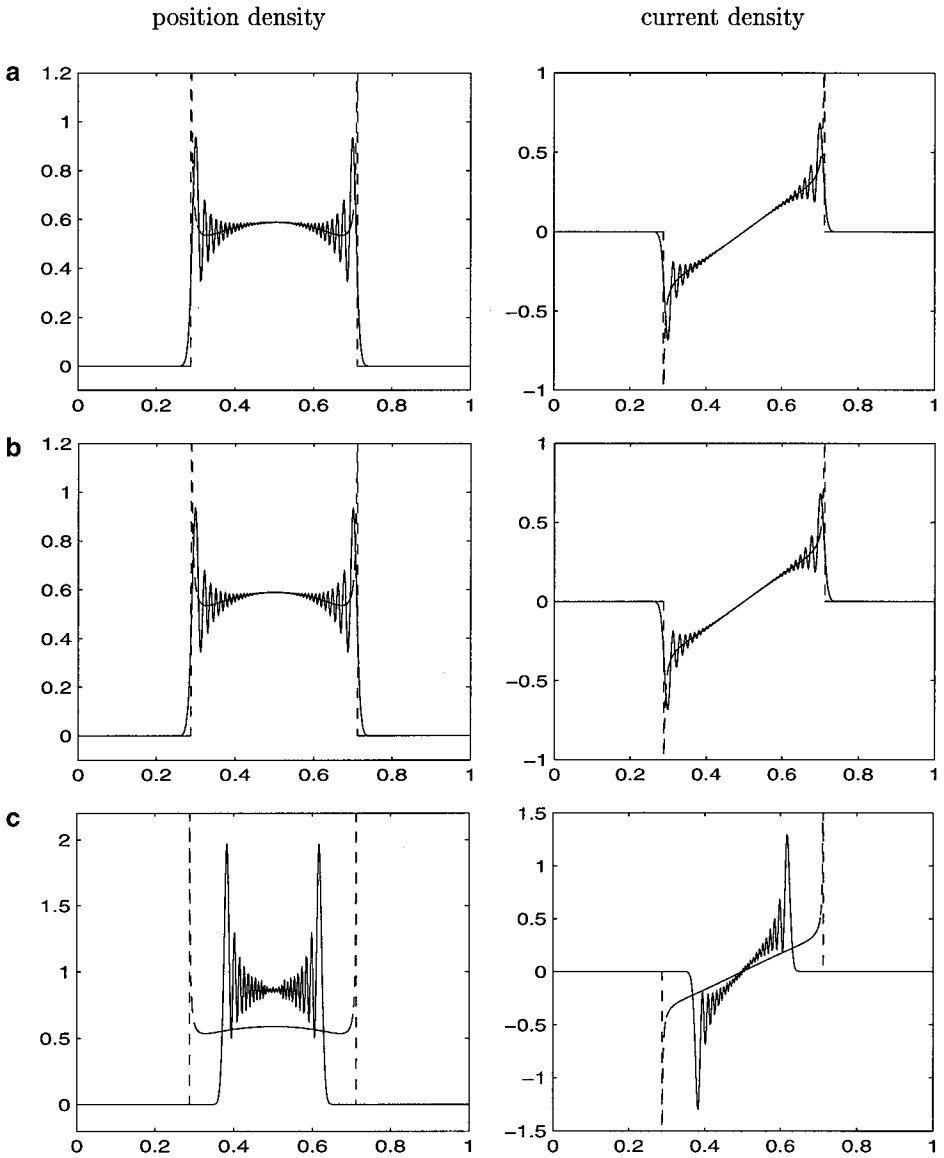
FIG. 3. Numerical solutions at $t = 0.54$ in Example 1. $\varepsilon = 10^{-3}$, $V(x) = 10$, $h = \frac{1}{512}$. (a) CNSP (2.13), $k = 0.00001$; (b) SP2 (2.9); (c) CNSP (2.13), $k = 0.0001$.

on the order of ε, while the finite difference approximation requires h to be much smaller than ε. This shows that the spectral approximation has much better spatial resolution for oscillatory solutions than the finite difference approximation. Our numerical experiments indicate that the meshing strategy for CNFD is

$$h = o(\varepsilon), \quad k = o(\varepsilon), \tag{7.5}$$

which was proved analytically and observed numerically in [14].

Last, we test the error estimate (3.10). For each fixed ε, we compute a numerical solution by using SP2 with a very fine mesh, e.g., $h = \frac{1}{32768}$, as the "exact" solution u^ε. Table I shows the errors $\|u^\varepsilon(t) - u^{\varepsilon,h}(t)\|_{l^2}$ at $t = 0.54$ for different ε and h.

TABLE I

The Error $\|u^\varepsilon(t) - u^{\varepsilon,h}(t)\|_{l^2}$ at $t = 0.54$ in Example 1

	Mesh					
	$h = \frac{1}{16}$	$h = \frac{1}{64}$	$h = \frac{1}{256}$	$h = \frac{1}{1024}$	$h = \frac{1}{4096}$	$h = \frac{1}{16384}$
$\varepsilon = 0.0256$	5.262E-3	4.087E-5	5.118E-6	6.431E-7	1.014E-7	6.268E-8
$\varepsilon = 0.0064$	0.4794	1.959E-4	1.770E-5	2.182E-6	2.773E-7	6.164E-8
$\varepsilon = 0.0016$	0.7374	0.5572	1.006E-4	8.748E-6	1.079E-6	1.433E-7
$\varepsilon = 0.0004$	0.6118	0.6940	0.4853	5.029E-5	4.368E-6	5.273E-7
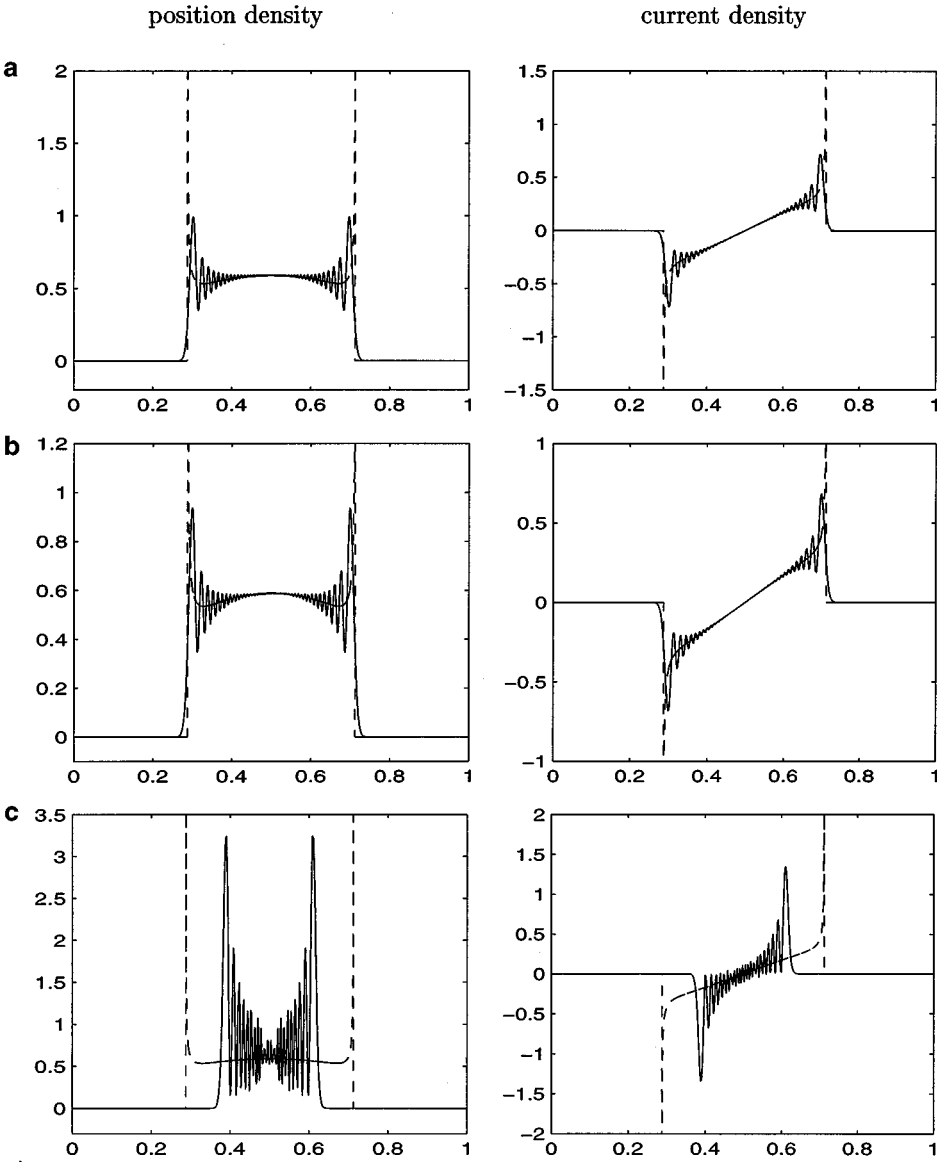
FIG. 4. Numerical solutions at $t = 0.54$ in Example 1. $\varepsilon = 10^{-3}$, $V(x) = 10$, $k = 0.00001$. (a) CNFD (2.16), $h = \frac{1}{4096}$; (b) CNSP (2.9), $h = \frac{1}{512}$; (c) CNFD (2.16), $h = \frac{1}{512}$.

As shown in Table I, the error $\|u^\varepsilon(t) - u^{\varepsilon,h}(t)\|_{l^2}$ goes to zero when $h = O(\varepsilon)$. Due to the oscillations of the initial data, when h is too large compared to ε, the error is large. This is because the numerical initial data (trigonometric interpolant) do not resolve the initial data in this case.

EXAMPLE 2.   The initial condition is taken as

$$n_0(x) = \left(e^{-25(x-0.5)^2}\right)^2, \quad S_0(x) = 0.2(x^2 - x). \tag{7.6}$$

This example was also used in [14, 15]. Caustics do not occur and the limiting position and current densities remain smooth. We solve this problem numerically on the interval [0, 1], i.e., $a = 0$ and $b = 1$ with periodic boundary conditions.

Let $V(x) = 100$ be the constant potential. The weak limits $n^0(x, t)$, $J^0(x, t)$ of $n^\varepsilon(x, t)$, $J^\varepsilon(x, t)$, respectively, as $\varepsilon \to 0$ at $t = 0.54$ are plotted in Fig. 5.

We perform tests similar to those in Example 1. Figures 6–8 show the corresponding results. Clearly, the same conclusion can be drawn as for Example 1.
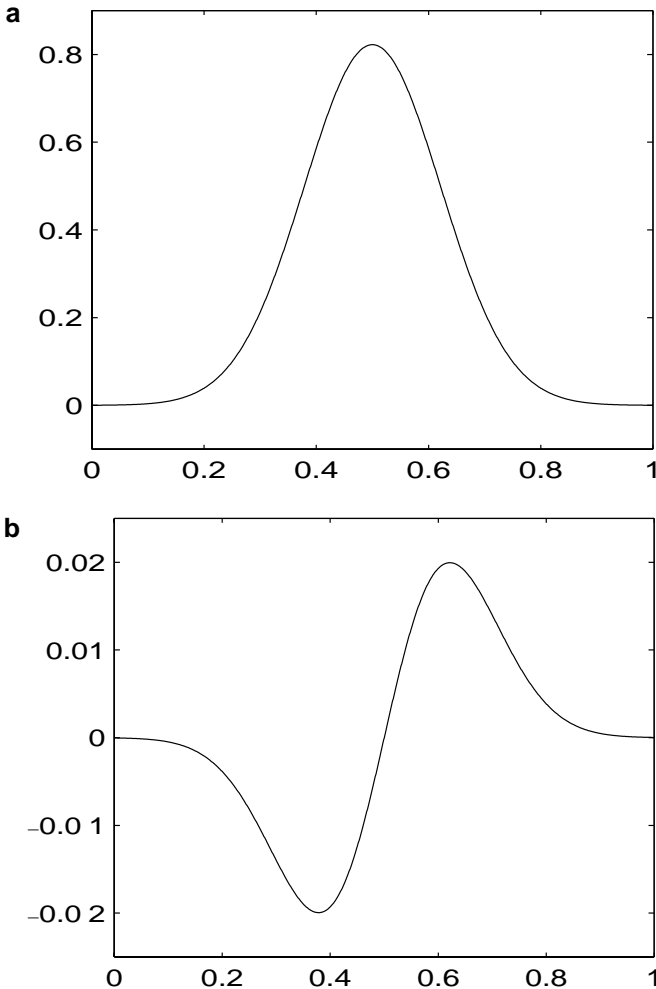

FIG. 5.   Weak limits in Example 2 at $t = 0.54$. (a) $n^0(x, 0.54)$; (b) $J^0(x, 0.54)$.

position density   current density
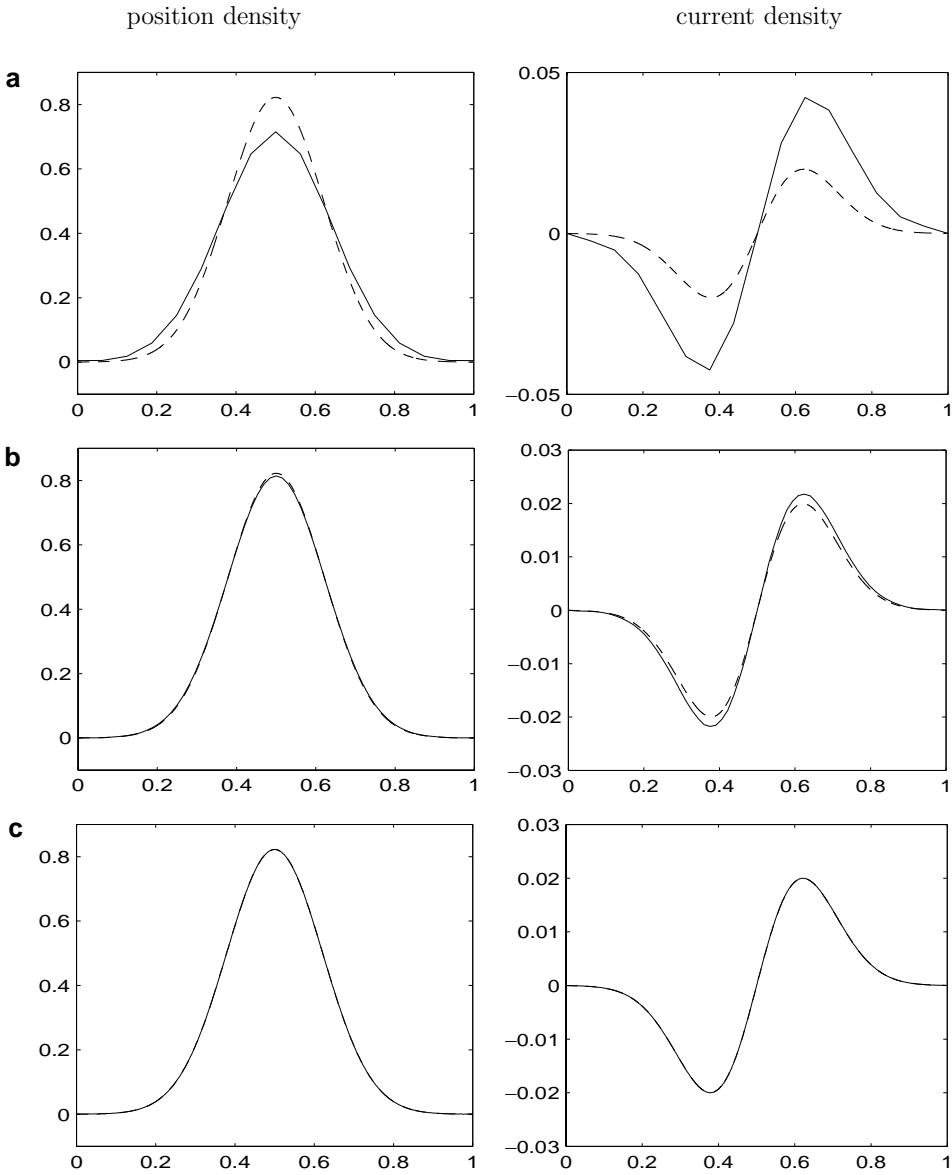

FIG. 6. Numerical solutions at $t = 0.54$ in Example 2 by using SP2 (2.9). $V(x) = 100$. (a) $\varepsilon = 0.0256$, $h = \frac{1}{16}$; (b) $\varepsilon = 0.0064$, $h = \frac{1}{64}$; (c) $\varepsilon = 0.0008$, $h = \frac{1}{512}$; (d) $\varepsilon = 0.0001$, $h = \frac{1}{4096}$; (e) $\varepsilon = 0.000025$, $h = \frac{1}{16384}$; (f) $\varepsilon = 0.0000125$, $h = \frac{1}{32768}$.

From the numerical results of these two examples, in which the potentials are constants, one can see that the time-splitting spectral approximation gives very promising results. The mesh size h can be chosen as $O(\varepsilon)$ and the time integration is exact, while for finite differences k has to be $o(\varepsilon)$.

In the next two examples, we perform tests on SP2 (2.9) for inhomogeneous potentials.

EXAMPLE 3.   The initial condition is taken as

$$n_0(x) = \left(e^{-25(x-0.5)^2}\right)^2, \quad S_0(x) = x + 1. \tag{7.7}$$
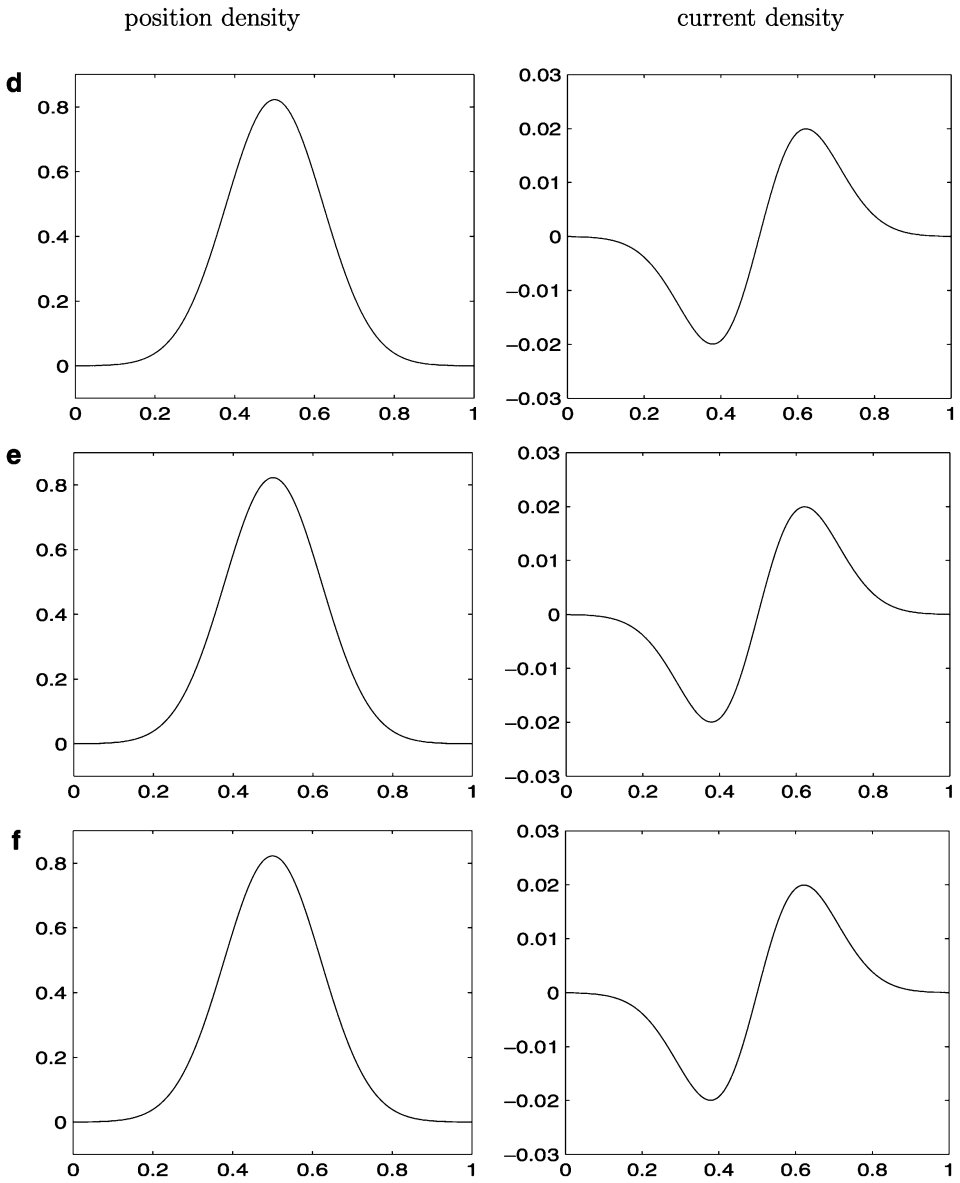
position density

current density

FIG. 6—*Continued*

Let $V(x) = \frac{x^2}{2}$, which is a harmonic oscillator. For this example, the weak limits $n^0(x, t)$ and $J^0(x, t)$ of $n^\varepsilon(x, t)$ and $J^\varepsilon(x, t)$, respectively, as $\varepsilon \to 0$ are given in Gasser and Markowich [7].

We solve the problem on the interval $[-2, 2]$ with periodic boundary conditions using SP2. Figure 9 shows the numerical results at $t = 0.52$, $t = 3.6$, and $t = 5.5$ with $k = 0.02$ when we choose $\varepsilon = 0.04$, $h = \frac{1}{16}$; $\varepsilon = 0.0025$, $h = \frac{1}{256}$; and $\varepsilon = 0.00015625$, $h = \frac{1}{4096}$. In all these runs, h is on the order of ε and k is chosen as constant independent of ε, yet the numerical solutions are very good approximations of the exact weak limit. This agrees with the analysis of Section 6.

We also test the error estimate (4.2). For each fixed ε, we compute a numerical solution by using SP2 with a very fine mesh, e.g., $h = \frac{1}{32768}$, and a very small time step, e.g.,

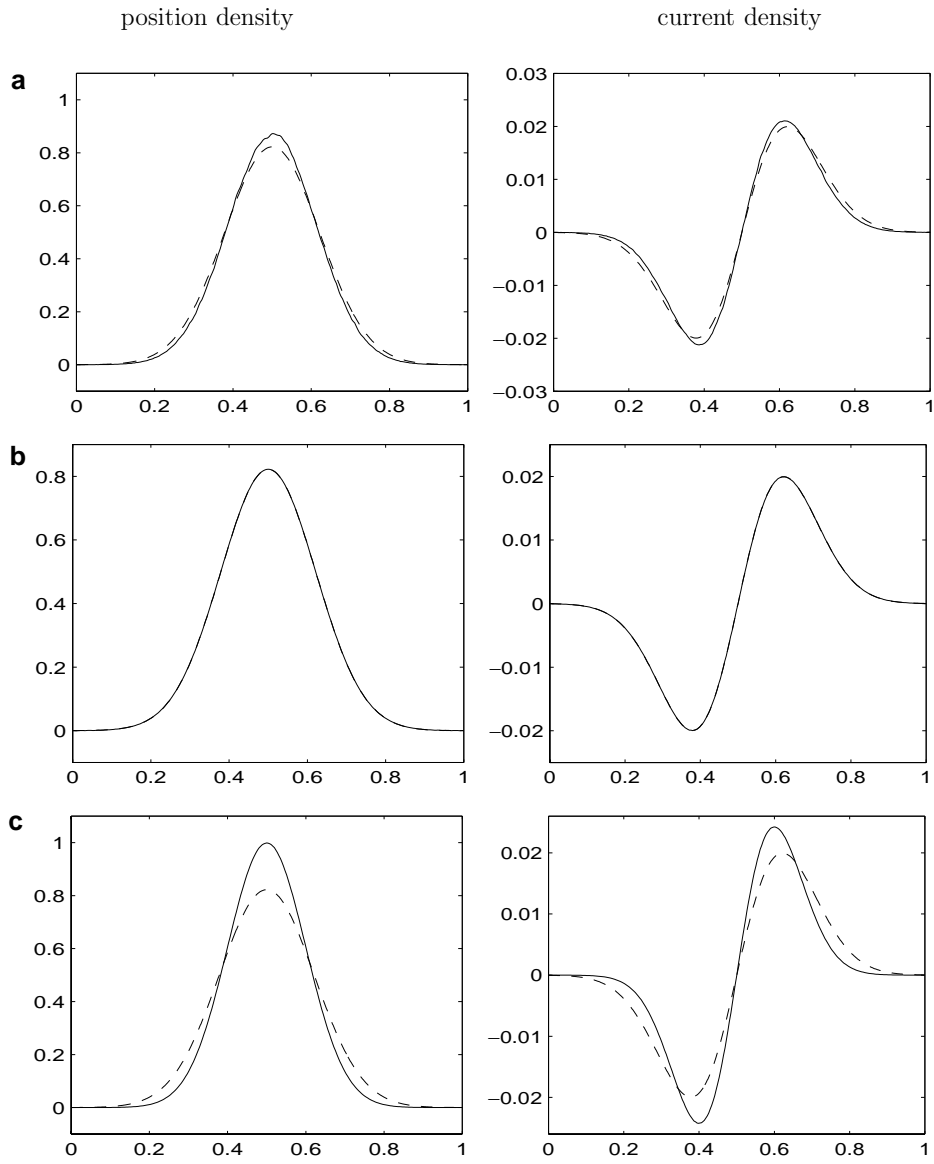position density   current density

FIG. 7. Numerical solutions at $t = 0.54$ in Example 2. $\varepsilon = 2.5 \times 10^{-4}$, $V(x) = 100$, $h = \frac{1}{256}$. (a) CNSP (2.16), $k = 0.000004$; (b) SP2 (2.9); (c) CNSP (2.16), $k = 0.0001$.

$k = 0.00001$, as the "exact" solution u^ε. Tables II–IV show the errors $\|u^\varepsilon(t) - u^{\varepsilon,h,k}(t)\|_{l^2}$ at $t = 0.64$ for different combinations of ε, h, and k.

As shown in Tables II–IV, the error $\|u^\varepsilon(t) - u^{\varepsilon,h,k}(t)\|_{l^2}$ converges for the meshing strategy $h = O(\varepsilon)$ and $k = O(\varepsilon)$.

EXAMPLE 4 (2-dimensional).   The initial condition is taken as

$$n_0(x, y) = \left(e^{-25[(x-0.5)^2 + 0.8(y-0.5)^2]}\right)^2, \quad S_0(x, y) = x + 0.5y. \tag{7.8}$$

TABLE II

The Error $\|u^\varepsilon(t) - u^{\varepsilon,h,k}(t)\|_{l^2}$ at $t = 0.64$ with $\varepsilon = 0.04$ in Example 3

	Mesh				
	$h = \frac{1}{4}$	$h = \frac{1}{16}$	$h = \frac{1}{64}$	$h = \frac{1}{256}$	$h = \frac{1}{1024}$
$k = 0.16$	0.7086	7.557E-3	7.556E-3	7.556E-3	7.556E-3
$k = 0.04$	0.7097	4.801E-4	4.697E-4	4.697E-4	4.697E-4
$k = 0.01$	0.7098	1.042E-4	2.935E-5	2.935E-5	2.935E-5
$k = 0.0025$	0.7098	1.000E-4	1.834E-6	1.834E-6	1.834E-6
$k = 0.000625$	0.7098	1.000E-4	1.146E-7	1.146E-7	1.146E-7
$k = 0.00015625$	0.7098	1.000E-4	7.230E-9	7.230E-9	7.136E-9
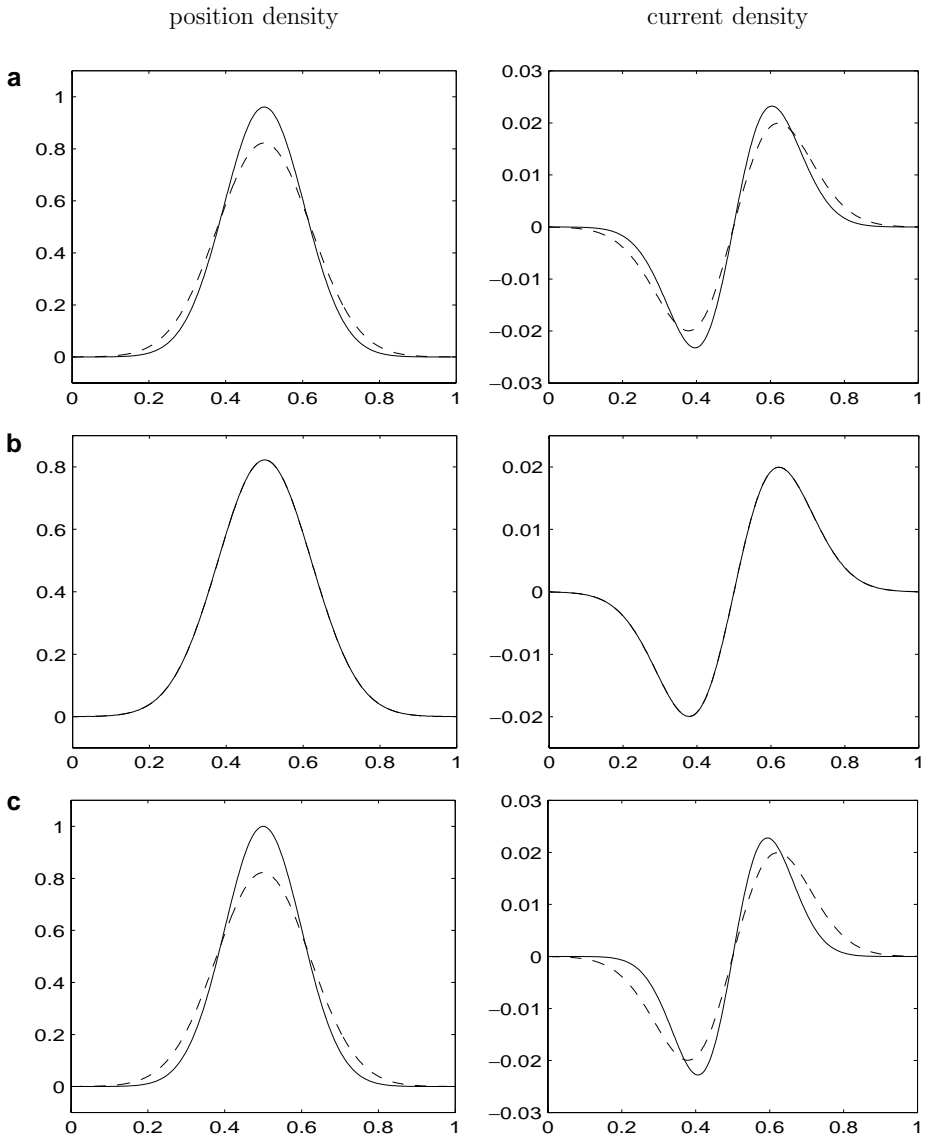
FIG. 8. Numerical solutions at $t = 0.54$ in Example 2. $\varepsilon = 2.5 \times 10^{-4}$, $V(x) = 100$. (a) CNFD (2.13), $h = \frac{1}{1024}$, $k = 0.00001$; (b) SP2 (2.9), $h = \frac{1}{256}$; (c) CNFD (2.13), $h = \frac{1}{256}$, $k = 0.0001$.
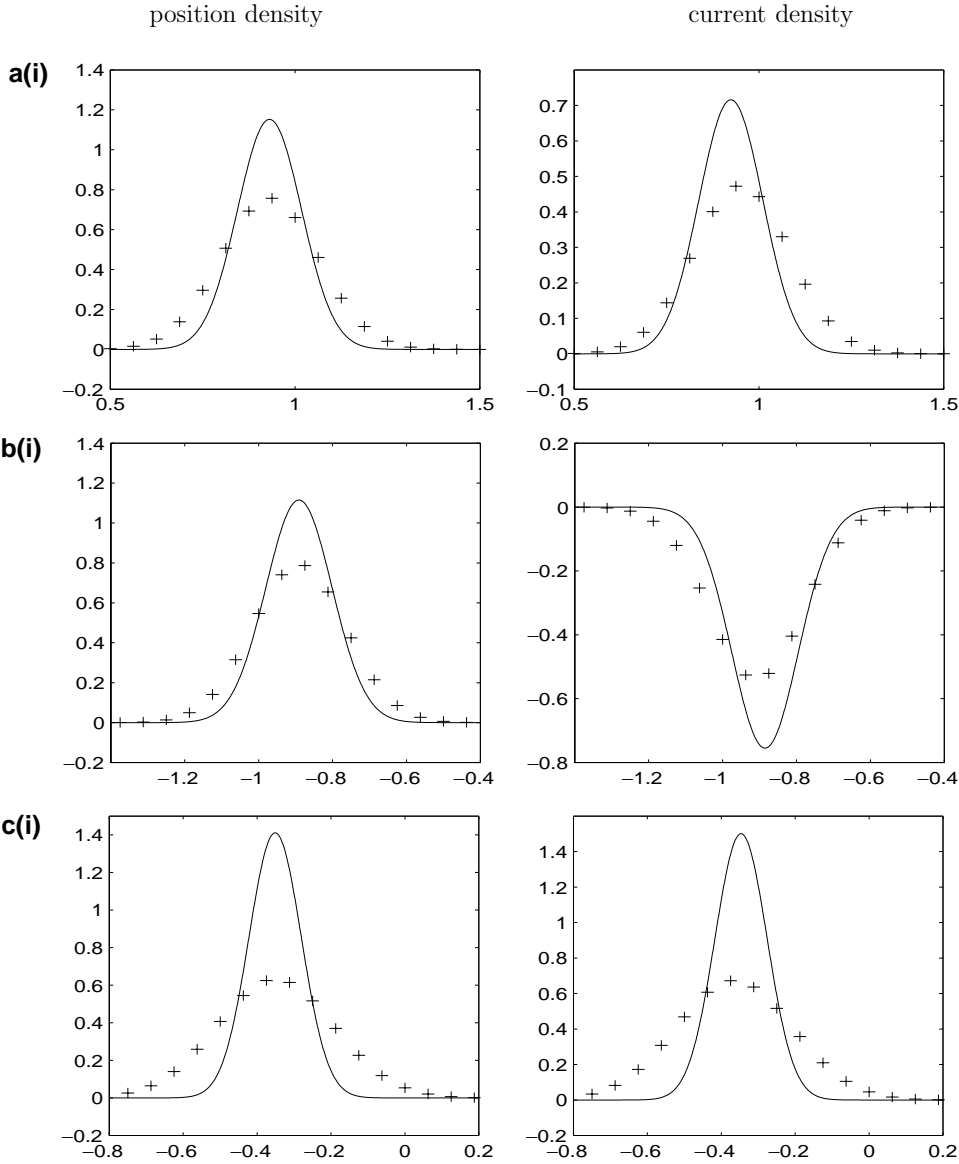
position density   current density

FIG. 9. Numerical solutions at different times in Example 3 by using SP2 (2.9). $k = 0.02$. +++: numerical solution, ———: weak limit. (a) $t = 0.52$; (b) $t = 3.6$; (c) $t = 5.5$. (i) $\varepsilon = 0.04$, $h = \frac{1}{16}$. (ii) $\varepsilon = 0.0025$, $h = \frac{1}{256}$. (iii) $\varepsilon = 0.00015625$, $h = \frac{1}{4096}$.

Let $V(x, y) = \frac{x^2 + y^2}{2}$, corresponding to the two-dimensional harmonic oscillator. For this example, the weak limits $n^0(x, y, t)$ and $\mathbf{J}^0(x, y, t)$ of $n^\varepsilon(x, y, t)$ and $\mathbf{J}^\varepsilon(x, y, t)$, respectively, as $\varepsilon \to 0$ are given in Gasser and Markowich [7].

We compute on the rectangle $[-2, 2] \times [-2, 2]$ with periodic boundary conditions. Figure 10 shows the numerical solutions on the lines $y = -0.25$ and $x = 0$ at $t = 2.7$, with $k = 0.05$ and different values of ε and mesh sizes h. Conclusions similar to those for the one-dimensional case can be made for the meshing strategy.

From these numerical results, we see that the numerical methods, SP2 (2.9) or SP1 (2.5), give very promising results on the observables in the semiclassical regime with

ε-independent time step k and mesh size $h = O(\varepsilon)$, in one and two space dimensions for the linear Schrödinger equation.

We shall now present numerical results for some nonlinear Schrödinger problems. However, we remark that these results can only be considered preliminary, with the goal of initiating the analysis of discretization techniques for the semiclassical regime in general and of the spectral time splitting techniques in particular. Much more research must be done in the analysis and numerical treatment of nonlinear Schrödinger equations with a small-scaled Planck constant.

FIG. 9—*Continued*

position density   current density

a(iii)

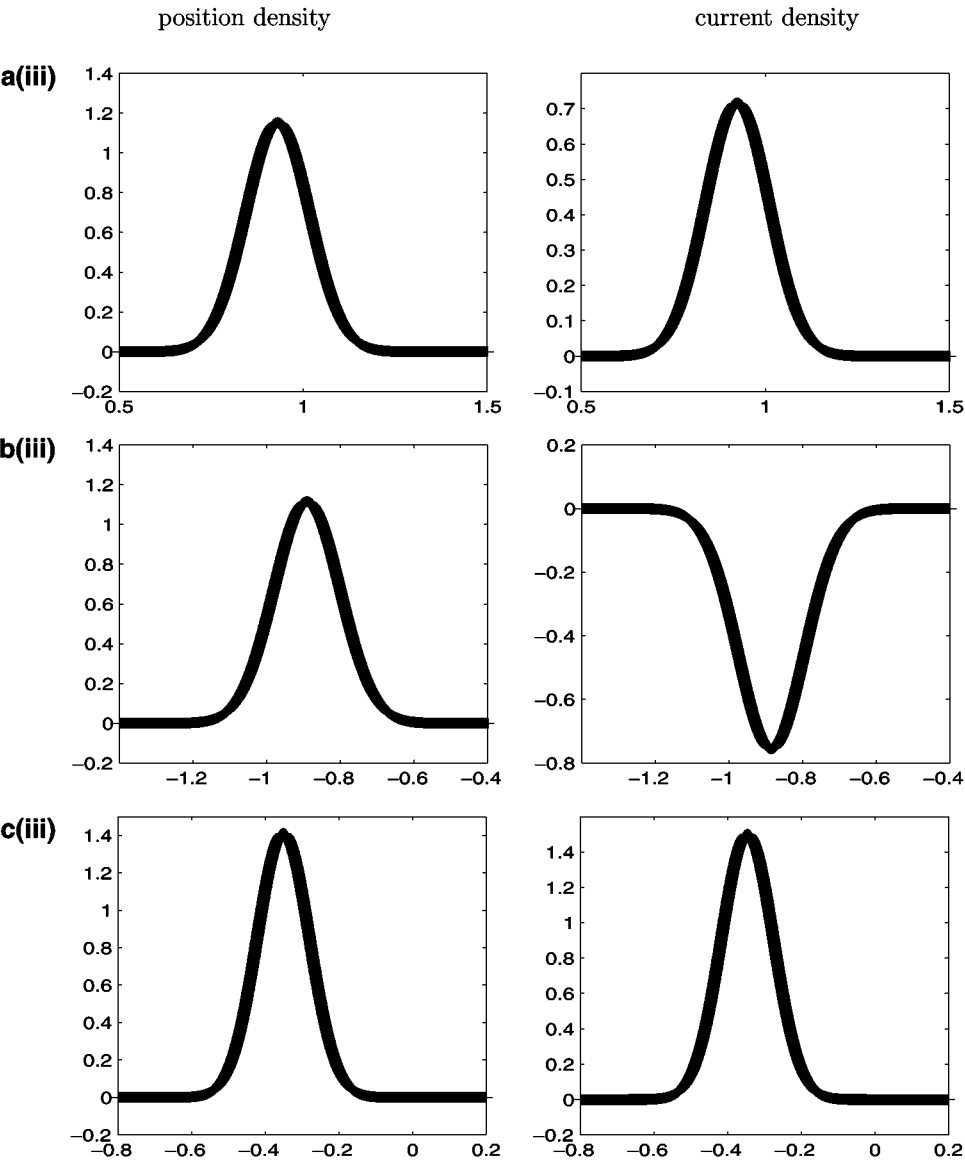**b(iii)**

c(iii)
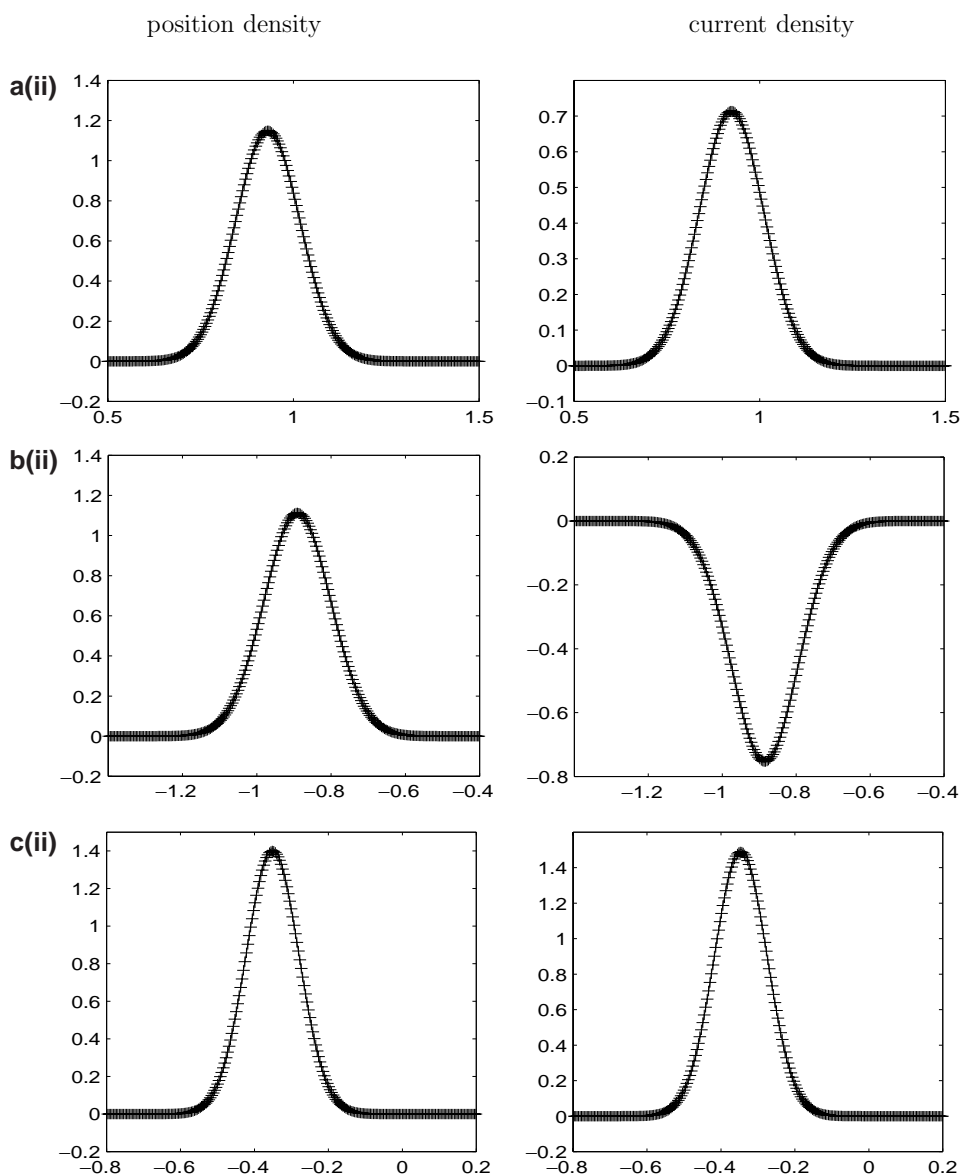
FIG. 9—*Continued*

In many applications nonlinear Schrödinger equations of the form

$$\varepsilon u_t^\varepsilon - i\frac{\varepsilon^2}{2}u_{xx}^\varepsilon + i\Phi^\varepsilon(x,t)u^\varepsilon = 0, \tag{7.9}$$

$$u^\varepsilon(x, t = 0) = u_I^\varepsilon(x) \tag{7.10}$$

appear, where the potential Φ^ε is given by

$$\Phi^\varepsilon(x,t) = \int \alpha V_0(x, y)|u^\varepsilon(y, t)|^2 \, dy + \beta_\varepsilon V_1(|u^\varepsilon(x, t)|^2). \tag{7.11}$$

TABLE III

The Error $\|u^\varepsilon(t) - u^{\varepsilon,h,k}(t)\|_{l^2}$ at $t = 0.64$ with $\varepsilon = 0.01$ in Example 3

	Mesh			
	$h = \frac{1}{16}$	$h = \frac{1}{64}$	$h = \frac{1}{256}$	$h = \frac{1}{1024}$
$k = 0.16$	0.7074	2.340E-2	2.340E-2	2.340E-2
$k = 0.04$	0.7076	1.454E-3	1.454E-3	1.454E-3
$k = 0.01$	0.7076	9.086E-5	9.086E-5	9.086E-5
$k = 0.0025$	0.7076	5.678E-6	5.678E-6	5.678E-6
$k = 0.000625$	0.7076	3.548E-7	3.548E-7	3.548E-7
$k = 0.00015625$	0.7076	2.209E-8	2.209E-8	2.209E-8

Here $0 \le V_0$ is a two-body long-range interaction potential (satisfying $V_0(x, y) = V_0(y, x)$, $\forall x, y \in \mathbb{R}$), and $V_1 \ge 0$ is the primitive of an entropy function (modeling short-range interactions). α and β_ε are real; $\alpha > 0$ corresponds to a repulsive long-range interaction, $\alpha < 0$ to an attractive one, $\beta_\varepsilon > 0$ is the defocusing case, and $\beta_\varepsilon < 0$ the focusing case.

The splitting method SP1 corresponds to solving, between $t = t_n$ and $t = t_{n+1}$,

$$u_t^\varepsilon = i\frac{\varepsilon}{2}u_{xx}^\varepsilon \qquad (7.12)$$

followed by

$$\varepsilon u_t^\varepsilon = -i\,\Phi^\varepsilon(x, t)u^\varepsilon. \qquad (7.13)$$

Also, for $t \in [t_n, t_{n+1}]$, the ODE (7.13) leaves $|u^\varepsilon|$ invariant in t,

$$\frac{\partial}{\partial t}(|u^\varepsilon|^2) = 2\,\mathrm{Re}\left(u_t^\varepsilon\,\overline{u^\varepsilon}\right) = -\frac{2}{\varepsilon}\,\mathrm{Re}(i\,\Phi^\varepsilon|u^\varepsilon|^2) = 0$$

(since Φ^ε is real valued). $|u^\varepsilon|$ becomes time-independent on $[t_n, t_{n+1}]$ (since Φ^ε only depends on $|u^\varepsilon|$) and therefore

$$\varepsilon u_t^\varepsilon = -i\,\Phi^\varepsilon(x, t_n)u^\varepsilon \qquad (7.14)$$

can be integrated exactly just as in the linear case.

TABLE IV

The Error $\|u^\varepsilon(t) - u^{\varepsilon,h,k}(t)\|_{l^2}$ at $t = 0.64$ with $\varepsilon = 0.0025$ in Example 3

	Mesh			
	$h = \frac{1}{64}$	$h = \frac{1}{256}$	$h = \frac{1}{1024}$	$h = \frac{1}{4096}$
$k = 0.16$	0.7080	9.153E-2	9.153E-2	9.153E-2
$k = 0.04$	0.7080	5.699E-3	5.699E-3	5.699E-3
$k = 0.01$	0.7080	3.560E-4	3.560E-4	3.560E-4
$k = 0.0025$	0.7080	2.225E-5	2.225E-5	2.225E-5
$k = 0.000625$	0.7080	1.390E-6	1.390E-6	1.390E-6
$k = 0.00015625$	0.7080	8.657E-8	8.657E-8	8.657E-8

position density   x − component current density
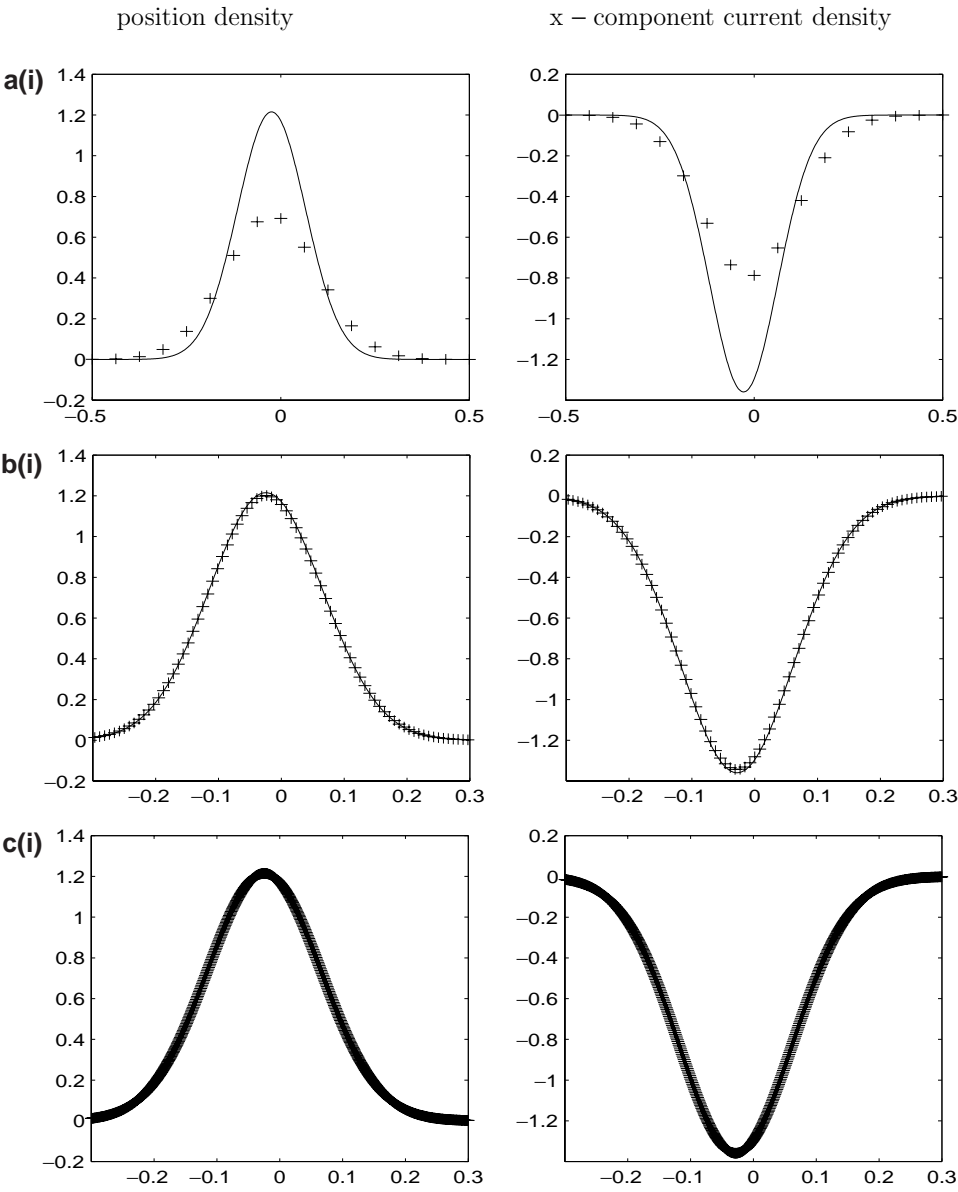

FIG. 10. Numerical solutions at $t = 2.7$ in Example 4 by using SP2 (2.9). $k = 0.05$. +++: numerical solution, ——: weak limit. (a) $\varepsilon = 0.04$; $h = \frac{1}{16}$; (b) $\varepsilon = 0.005$, $h = \frac{1}{128}$; (c) $\varepsilon = 0.000625$, $h = \frac{1}{1024}$. (i) On the line $y = 0.0$. (ii) On the line $x = -0.25$.

Similarly, SP2 can be formulated for this class of nonlinear problems, again doing all t-integrations exactly after spectral discretization in space.

EXAMPLE 5 (attractive Schrödinger–Poisson equation). Consider the nonlinear IVP (7.9), (7.10) subject to periodic boundary condition on $[a, b]$. Let $\alpha = -1$, $\beta_\varepsilon = 0$, and let V_0 be the Green function of the operator $-\frac{d^2}{dx^2}$ subject to homogeneous Dirichlet boundary conditions in (7.11).
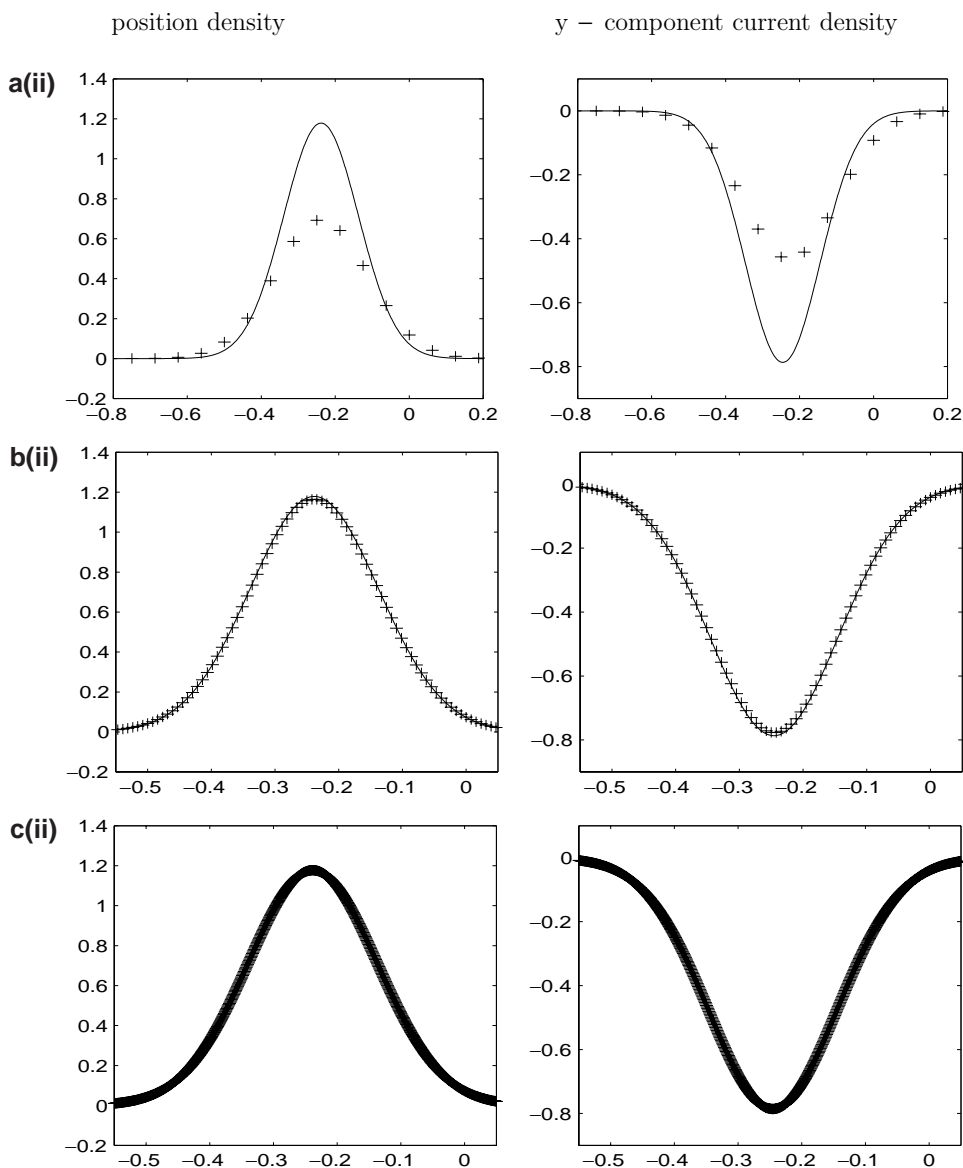
position density   y − component current density

FIG. 10—*Continued*

The initial condition is taken as

$$u_I^\varepsilon(x) = A(x)e^{iS(x)/\varepsilon}, \quad A(x) = e^{-x^2}, \quad S(x) = -\ln(e^x + e^{-x}), \tag{7.15}$$

and we choose $a = -4$, $b = 4$. To test the numerical method, for each fixed ε, we compute an approximate solution by using SP2 with a very fine mesh, e.g., $h = \frac{1}{4096}$, and a very small time step, e.g., $k = 0.0001$, as the "exact" solution u^ε. Figure 11 shows the numerical results at $t = 1.5$ with $k = 0.01$ when we choose $\varepsilon = 0.08$, $h = \frac{1}{16}$; $\varepsilon = 0.01$, $h = \frac{1}{128}$; $\varepsilon = 0.00125$, $h = \frac{1}{1024}$. In Fig. 11 as well as Figs. 12 and 13, the solid line is the "exact" solution and the +++ line is the numerically obtained solution. To obtain a better visualization
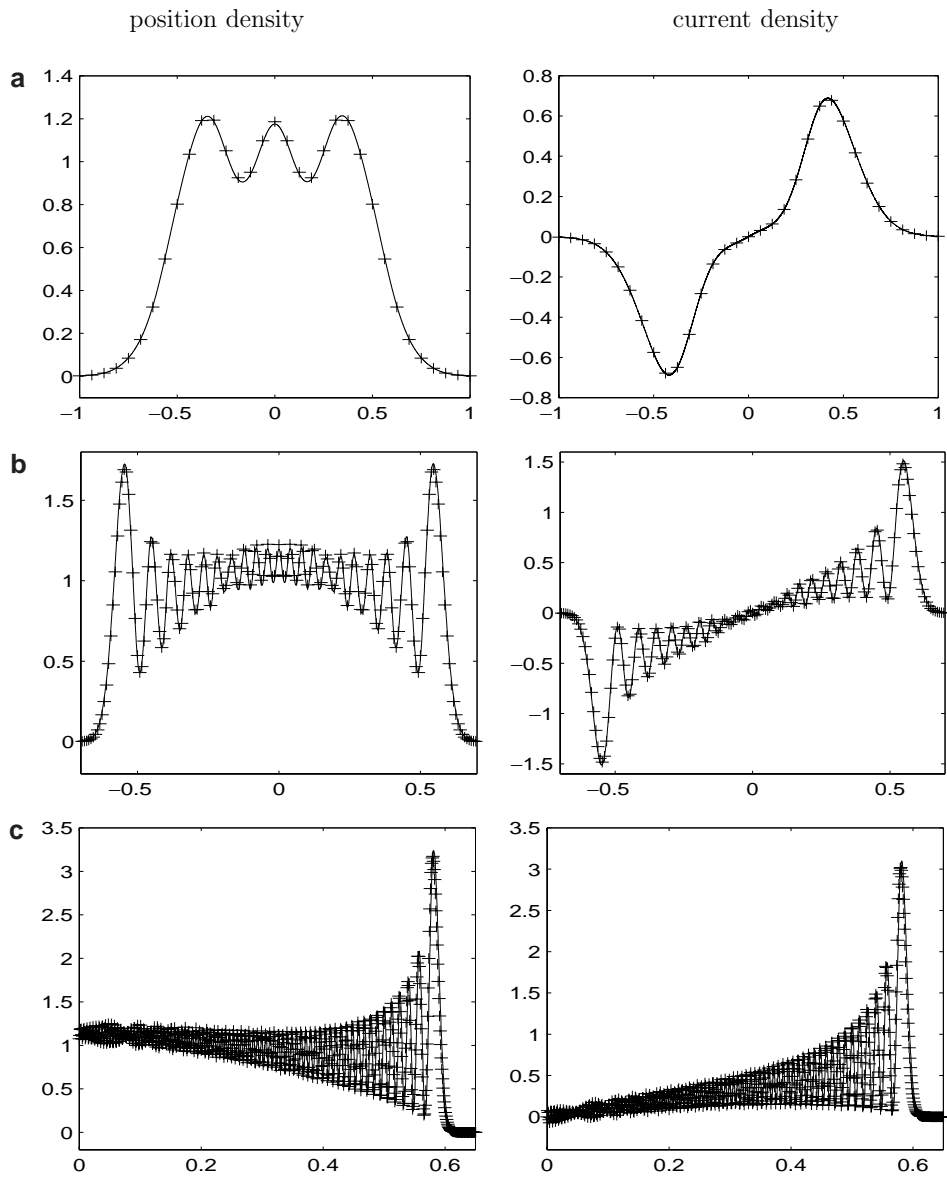
position density   current density

FIG. 11. Numerical solutions at $t = 1.5$ in Example 5 by using SP2. $k = 0.01$. +++: numerical solution, ——: "exact" solution. (a) $\varepsilon = 0.08$, $h = \frac{1}{16}$; (b) $\varepsilon = 0.01$, $h = \frac{1}{128}$; (c) $\varepsilon = 0.00125$, $h = \frac{1}{1024}$.

in these figures, we depict the solutions in a subinterval instead of in the whole computational interval $[-4, 4]$.

From Fig. 11 we can see that time-splitting spectral methods, SP2 and SP1, give very promising results in the semiclassical regime for ε-independent time step k when the spatial mesh size h is chosen as $O(\varepsilon)$, i.e., just as for the linear Schrödinger equation.

EXAMPLE 6 (nonlinear Schrödinger equation). Consider the nonlinear Schrödinger equation (7.9) with $\alpha = 0$, defocusing strong $O(1)$ nonlinearity, e.g., $\beta_\varepsilon = 1$ or focus-
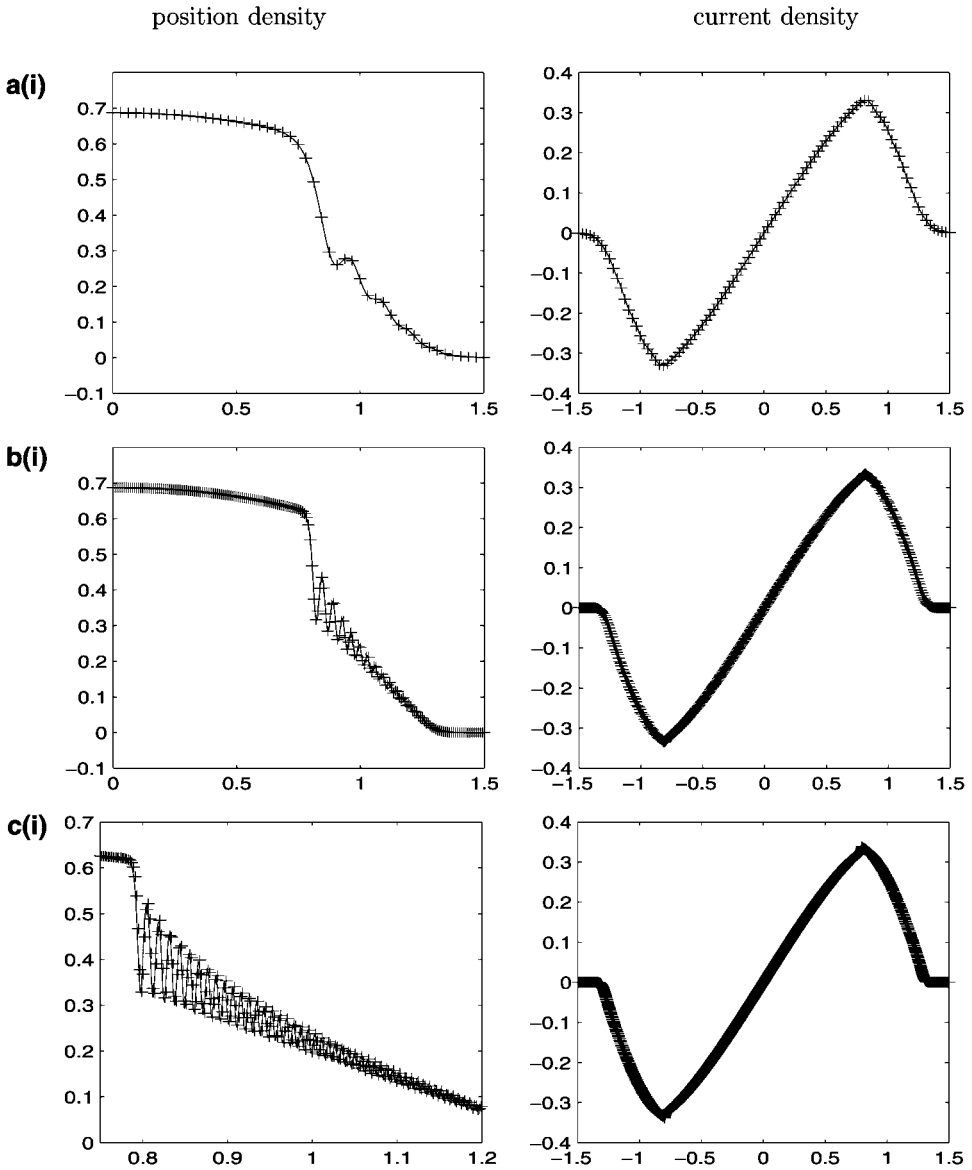
position density　　　　　　　　current density

a(i)

b(i)

c(i)

FIG. 12. Numerical solutions at $t = 1.0$ in Example 6 by using SP2 for defocusing nonlinearity $\beta_\varepsilon = 1.0$. +++: numerical solution, ——: "exact" solution. (i) Under meshing strategy: $h = O(\varepsilon)$ and $k = O(\varepsilon)$: (a) $\varepsilon = 0.04$, $k = 0.008$, $h = \frac{1}{32}$; (b) $\varepsilon = 0.01$, $k = 0.002$, $h = \frac{1}{128}$; (c) $\varepsilon = 0.0025$, $k = 0.0005$, $h = \frac{1}{512}$. (ii) Under meshing strategy: $h = O(\varepsilon)$ and $k = 0.008$-independent of ε: (a) $\varepsilon = 0.04$, $k = 0.008$, $h = \frac{1}{32}$; (b) $\varepsilon = 0.01$, $k = 0.008$, $h = \frac{1}{128}$; (c) $\varepsilon = 0.0025$, $k = 0.008$, $h = \frac{1}{512}$.

ing weak $O(\varepsilon)$ nonlinearity, e.g., $\beta_\varepsilon = -\varepsilon$ in (7.11). Also, set $V_1(s) = s$; i.e., we deal with the cubically nonlinear Schrödinger equation. This problem was studied in, e.g., [2, 11, 12].

For the defocusing case, e.g., $\beta_\varepsilon = 1$, the initial condition is taken ε-oscillatory:

$$u_I^\varepsilon(x) = A(x)e^{iS(x)/\varepsilon}, \quad A(x) = e^{-x^2}, \quad S(x) = -\ln(e^x + e^{-x}). \tag{7.16}$$

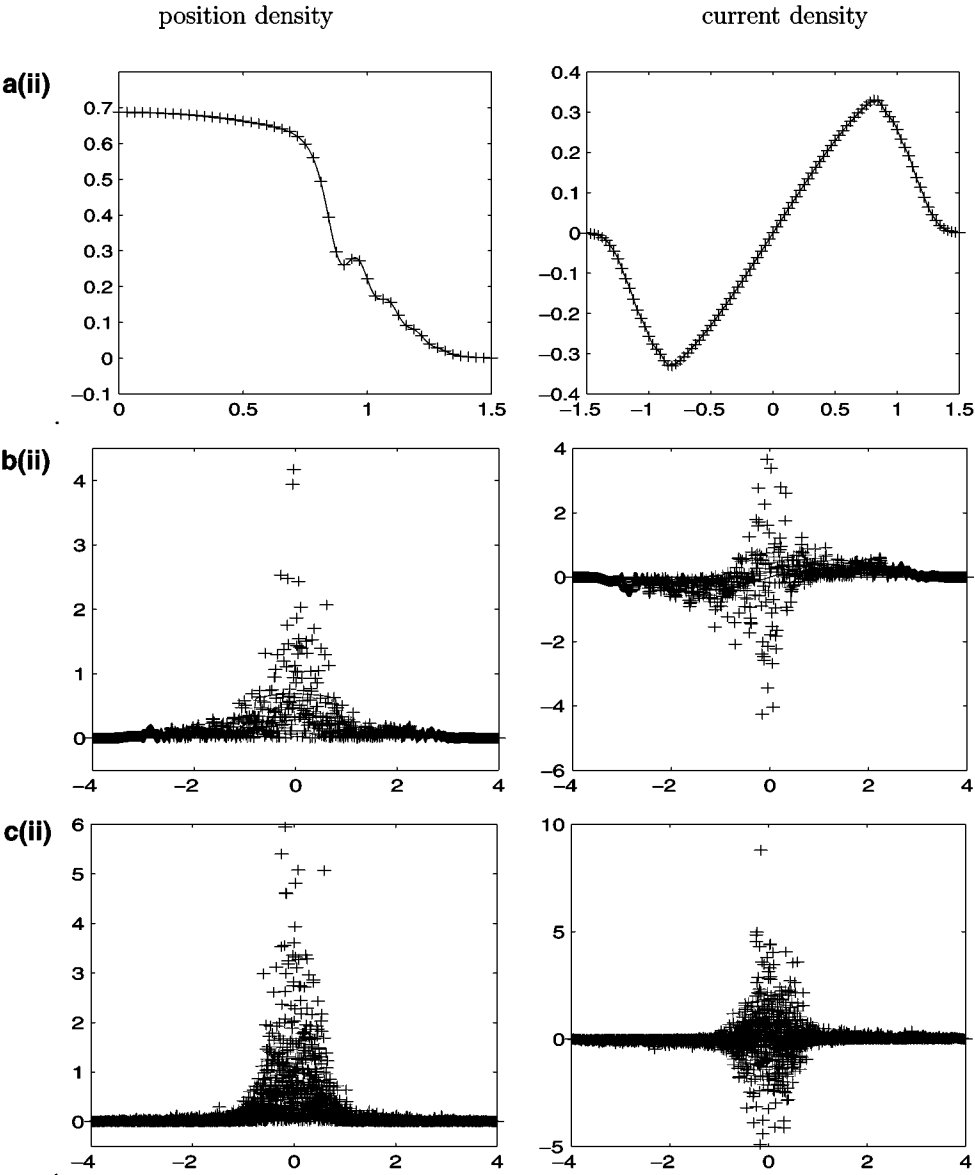position density   current density

FIG. 12—*Continued*

We solve the problem on the interval $[-4, 4]$ with periodic boundary conditions. To test the numerical method, for each fixed ε, we compute a numerical solution by using SP2 with a very fine mesh, e.g., $h = \frac{1}{4096}$, and a very small time step, e.g., $k = 0.00001$, as the "exact" solution u^ε. Figure 12 shows the numerical results at $t = 1.0$ (after the caustics formed) with $\beta_\varepsilon = 1.0$ when we choose $\varepsilon = 0.04$, $k = 0.008$, $h = \frac{1}{32}$; $\varepsilon = 0.01$, $k = 0.002$, $h = \frac{1}{128}$; $\varepsilon = 0.0025$, $k = 0.0005$, $h = \frac{1}{512}$, which corresponds to the meshing strategy $h = O(\varepsilon)$ and $k = O(\varepsilon)$; and choosing $\varepsilon = 0.04$, $k = 0.008$, $h = \frac{1}{32}$; $\varepsilon = 0.01$, $k = 0.008$, $h = \frac{1}{128}$; $\varepsilon = 0.0025$, $k = 0.008$, $h = \frac{1}{512}$, which corresponds to the meshing strategy $h = O(\varepsilon)$ and $k = 0.008$-independent of ε.

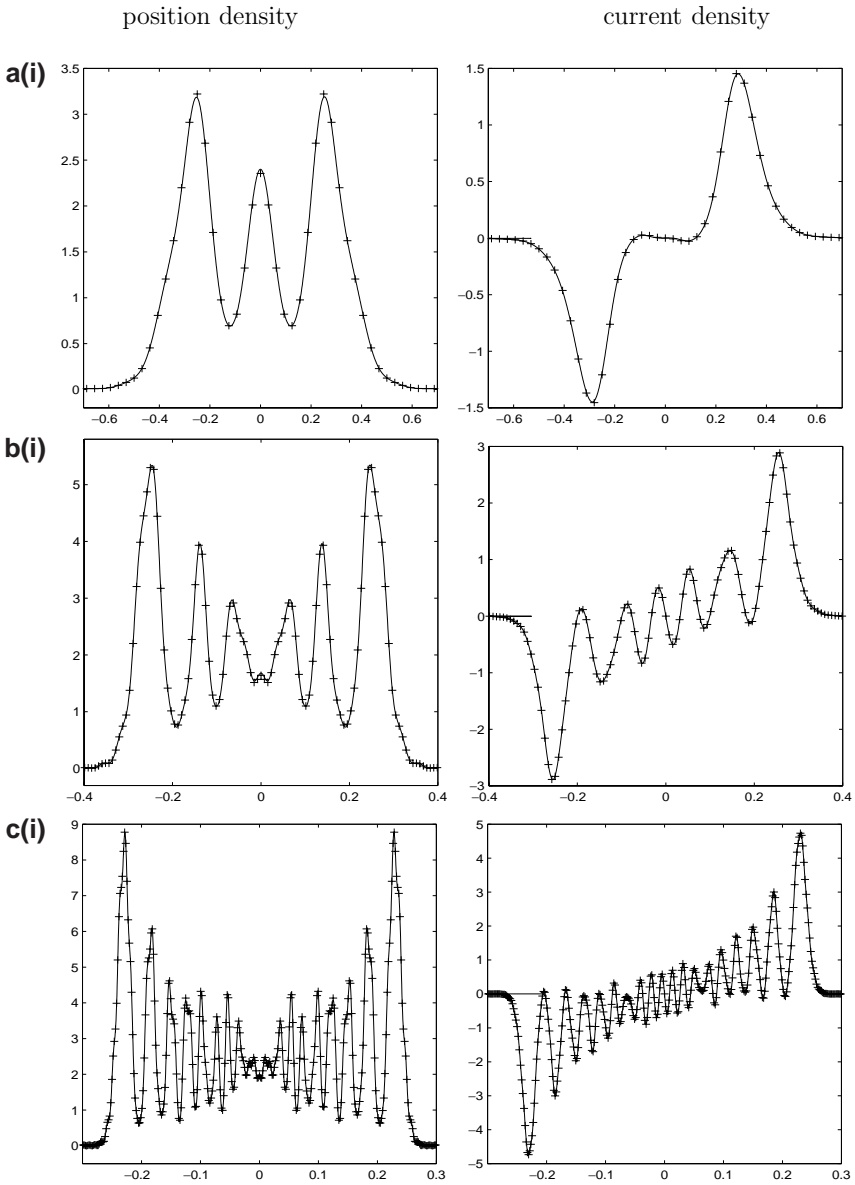position density   current density

FIG. 13. Numerical solutions at $t = 1.5$ in Example 6 by using SP2 for focusing weak $O(\varepsilon)$ nonlinearity $\beta_\varepsilon = -\varepsilon$. +++: numerical solution, ——: "exact" solution. (i). Under meshing strategy: $h = O(\varepsilon)$ and $k = O(\varepsilon)$: (a) $\varepsilon = 0.04$, $k = 0.02$, $h = \frac{1}{32}$; (b) $\varepsilon = 0.01$, $k = 0.005$, $h = \frac{1}{128}$; (c) $\varepsilon = 0.0025$, $k = 0.00125$, $h = \frac{1}{512}$. (ii). Under meshing strategy: $h = O(\varepsilon)$ and $k = 0.02$-independent of ε: (a) $\varepsilon = 0.04$, $k = 0.02$, $h = \frac{1}{32}$; (b) $\varepsilon = 0.01$, $k = 0.02$, $h = \frac{1}{128}$; (c) $\varepsilon = 0.0025$, $k = 0.02$, $h = \frac{1}{512}$.

For the focusing weak $O(\varepsilon)$ nonlinearity case, e.g., $\beta_\varepsilon = -\varepsilon$, the initial condition is taken as

$$u_I^\varepsilon(x) = A(\varepsilon, x)e^{iS(x)/\varepsilon}, \quad A(\varepsilon, x) = \left(1 + 0.2\cos^2\left(\frac{x}{\sqrt{\varepsilon}}\right)\right)e^{-x^2},$$

$$S(x) = -\ln(e^x + e^{-x}). \tag{7.17}$$

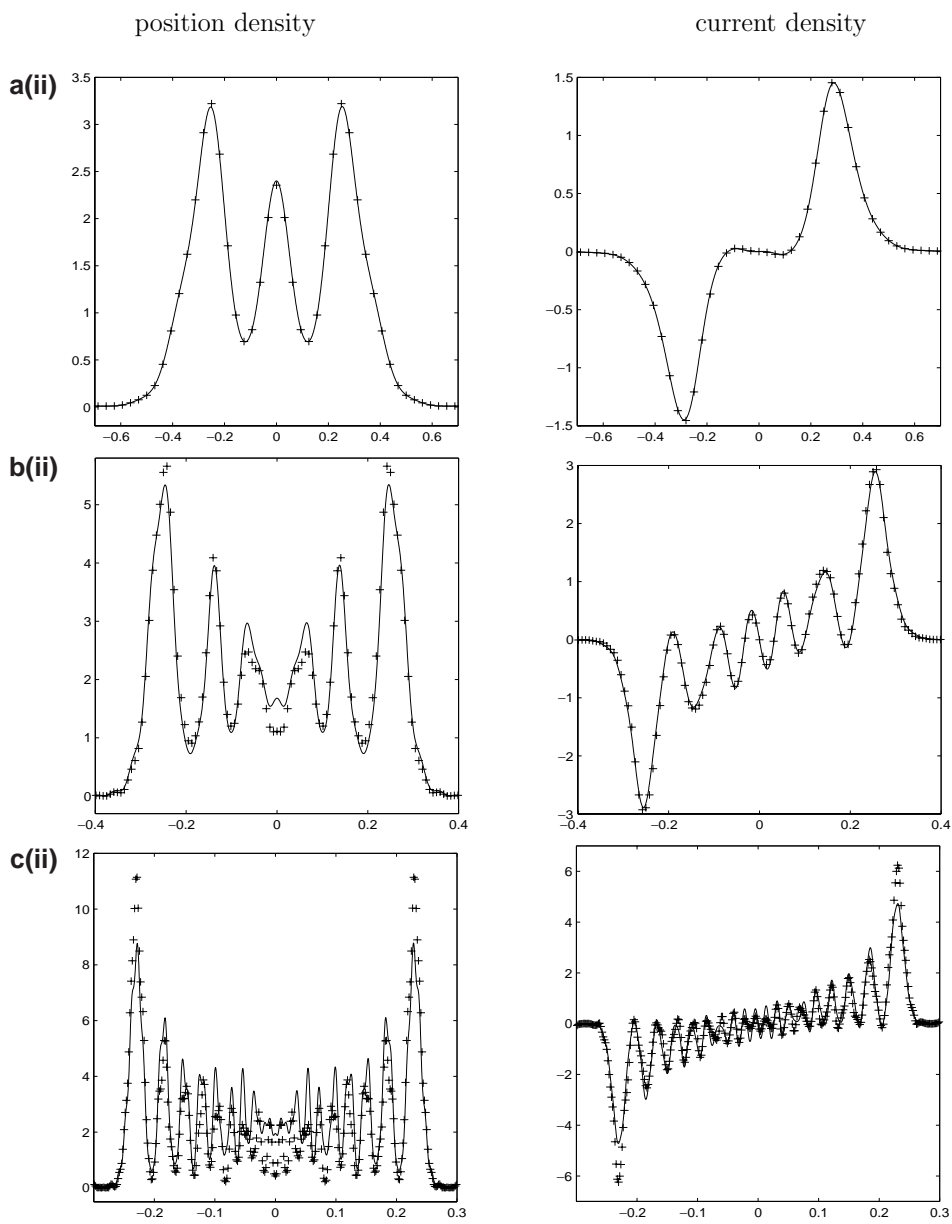position density   current density

FIG. 13—*Continued*

In fact, in these initial data, physically it has three scales: (i) x-laboratory scale; (ii) x/ε, the scale of the rapid oscillations; and (iii) an intermediate $x/\sqrt{\varepsilon}$ scale of the instability [2]. Similarly, the problem is solved on $[-4, 4]$ with periodic boundary conditions and the "exact" solution u^ε is obtained the same way as in the defocusing case. Figure 13 shows the numerical results at $t = 1.5$ (after the caustics formed) with $\beta_\varepsilon = -\varepsilon$ when we choose $\varepsilon = 0.04, k = 0.02, h = \frac{1}{32}; \varepsilon = 0.01, k = 0.005, h = \frac{1}{128}; \varepsilon = 0.0025, k = 0.00125, h = \frac{1}{512}$, which is $h = O(\varepsilon)$ and $k = O(\varepsilon)$; and for $\varepsilon = 0.04, k = 0.02, h = \frac{1}{32}; \varepsilon = 0.01, k = 0.02$, $h = \frac{1}{128}; \varepsilon = 0.0025, k = 0.02, h = \frac{1}{512}$, which is $h = O(\varepsilon)$ and $k = 0.02$-independent of ε.

From Figs. 12 and 13 we can see that one needs the following constraint in order to guarantee good approximations of all (smooth) observables for ε small: for the defocusing nonlinearity and focusing weak $O(\varepsilon)$ nonlinearity, i.e., $\beta_\varepsilon > 0$ and $\beta_\varepsilon = O(\varepsilon) < 0$ in (7.11), respectively, the meshing strategy is

$$h = O(\varepsilon), \quad k = O(\varepsilon). \tag{7.18}$$

Weaker constraint on meshing, e.g., $h = O(\varepsilon)$ and k-independent of ε, gives incorrect numerical observables.

Remark 7.1. For the focusing weak $O(\varepsilon)$ nonlinearity, e.g., $\beta_\varepsilon = -\varepsilon$, when the initial condition (7.16) is used, the constraint on the time step k and mesh size h is the same as in (7.18).

Remark 7.2. For the focusing strong $O(1)$ nonlinearity, e.g., $\beta_\varepsilon = -1$, due to the modulational instability (see detail in [2]), more study is required for this case.

8. CONCLUSIONS

Time-splitting spectral approximations for the Schrödinger equation in the semiclassical regime (i.e., for small-scaled Planck constant ε) were studied. They are based on a time-splitting method coupled with the trigonometric spectral approximation of the spatial derivative. This method conserves the total charge, and it is gauge-invariant, time-reversible, and very effective in capturing ε-oscillatory solutions of the Schrödinger equation in the small-Planck-constant regime. It allows the use of ε-independent time steps and a spatial mesh size comparable to the scaled Planck constant for the linear Schrödinger equation and for the weakly nonlinear Schrödinger–Poisson problem if only accurate quadratic observables are desired, while the frequently used finite difference methods require mesh size and time step much smaller than the scaled Planck constant ε. Numerical results for the nonlinear Schrödinger equation are also presented. In general, more restrictive meshing conditions are needed there.

Finally, we mention that extensive numerical study on this time-splitting spectral approximation for nonlinear Schrödinger equations has been recently carried out by the authors in [1].

REFERENCES

1. W. Bao, S. Jin, and P. A. Markowich, Numerical study of time-splitting spectral discretizations of nonlinear Schrödinger equations in the semi-clasical regimes, submitted for publication.

2. J. C. Bronski and D. W. McLaughlin, Semiclassical behavior in the NLS equation: Optical shocks—focusing instabilities, in *Singular Limits of Dispersive Waves* (Plenum, New York, London, 1994).

3. T. F. Chan, D. Lee, and L. Shen, Stable explicit schemes for equations of the Schrödinger type, *SIAM J. Numer. Anal.* **23**, 274 (1986).

4. T. F. Chan and L. Shen, Stability analysis of difference scheme for variable coefficient Schrödinger type equations, *SIAM J. Numer. Anal.* **24**, 336 (1987).

5. B. Desjardins, C. K. Lin, and T. C. Tso, Semiclassical limit of the derivative nonlinear Schrödinger equation, *M^3AS* **10**, 261 (2000).

6. A. Fannjiang, Shi Jin, and G. Papanicolaou, High frequency behavior of the focusing nonlinear Schrödinger equation with random inhomogeneities, *SIAM J. Appl. Math.*, in press.

7. I. Gasser and P. A. Markowich, Quantum hydrodynamics, Wigner transforms and the classical limit, *Asymptotic Anal.* **14**, 97 (1997).

8. P. Gérard, Microlocal defect measures, *Comm. PDE.* **16**, 1761 (1991).

9. P. Gérard, P. A. Markowich, N. J. Mauser, and F. Poupaud, Homogenization limits and Wigner transforms, *Comm. Pure Appl. Math.* **50**, 321 (1997).

10. D. Gottlieb and S. A. Orszag, *Numerical Analysis of Spectral Methods* (Soc. for Industr. & Appl. Math., Philadelphia, 1977).

11. Shan Jin, C. D. Levermore, and D. W. McLaughlin, The semiclassical limit of the defocusing NLS hierarchy, *Comm. Pure Appl. Math.* **LII**, 613 (1999).

12. Shan Jin, C. D. Levermore, and D. W. McLaughlin, The behavior of solutions of the NLS equation in the semiclassical limit, in *Singular Limits of Dispersive Waves* (Plenum, New York, London, 1994).

13. P. A. Markowich, N. J. Mauser, and F. Poupaud, A Wigner function approach to semiclassical limits: Electrons in a periodic potential, *J. Math. Phys.* **35**, 1066 (1994).

14. P. A. Markowich, P. Pietra, and C. Pohl, Numerical approximation of quadratic observables of Schrödinger-type equations in the semi-classical limit, *Numer. Math.* **81**, 595 (1999).

15. P. A. Markowich, P. Pietra, C. Pohl, and H. P. Stimming, *A Wigner-Measure Analysis of the Dufort-Frankel Scheme for the Schrödinger Equation*, preprint.

16. P. D. Miller and S. Kamvissis, On the semiclassical limit of the focusing nonlinear Schrödinger equation, *Phys. Lett. A* **247**, 75 (1998).

17. J. E. Pasciak, Spectral and pseudo-spectral methods for advection equations, *Math. Comp.* **35**, 1081 (1980).

18. D. Pathria and J. L. Morris, Pseudo-spectral solution of nonlinear Schrödinger equation, *J. Comput. Phys.* **87**, 108 (1990).

19. L. Tartar, H-measures: A new approach for studying homogenization, oscillations and concentration effects in partial differential equations, *Proc. Roy. Soc. Edinburgh Sect. A* **115**, 193 (1990).